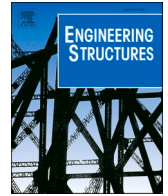# VICTORIA UNIVERSITY
MELBOURNE AUSTRALIA

Predicting the web crippling capacity of cold-formed steel lipped channels using hybrid machine learning techniques

This is the Published version of the following publication

Predicting the web crippling capacity of cold-formed steel lipped channels using hybrid machine learning techniques

Ramy I. Shahin [a], Mizan Ahmed [b], Qing Quan Liang [c],[*],[1], Saad A. Yehia [a]

[a] *Department of Civil Engineering, Higher Institute of Engineering and Technology, Kafrelsheikh, Egypt*
[b] *Centre for Infrastructure Monitoring and Protection, School of Civil and Mechanical Engineering, Curtin University, Kent Street, Bentley, WA 6102, Australia*
[c] *College of Sport, Health, and Engineering, Victoria University, PO Box 14428, Melbourne, VIC 8001, Australia*

A B S T R A C T

Cold-Formed Steel Lipped (CFSL) channels are susceptible to a localized failure mechanism known as web crippling, triggered by concentrated loads or reactions applied to the web of the section. These loads induce buckling and distortion in the web, ultimately leading to the member's collapse. It is a challenging task to accurately determine the web crippling capacity of a CFSL channel due to its complexity and various influencing factors. This paper presents hybrid soft computing techniques for accurately predicting the web crippling capacity of CFSL channels subjected to two flange load cases. The developed soft computing techniques combine Artificial Neural Networks (ANN) with either Genetic Algorithms (GA) or Particle Swarm Optimization (PSO) to improve computational efficiency and accuracy. The finite element models of CFSL channels are developed and validated by experimental results and then employed to generate a database, which is used to train machine learning models, including ANN, GA-ANN, and PSO-ANN. Analysis is undertaken on the reliability of existing design formulas for determining the web crippling capacity of CFSL channels. It is shown that the PSO-ANN model outperforms the other models in terms of prediction accuracy. The existing design codes and formulas are not reliable in estimating the web crippling capacity of CFSL channels. However, the proposed model yields good correlation with finite element analysis results. A user-friendly graphical interface tool is developed for the practical design of cold-formed steel lipped channels.

1. Introduction

Thin-walled Cold-Formed (CF) section members are manufactured from flat steel sheets or strips by cold-forming processes at ambient temperature to create the desired shape such as C-channels, Z-sections, and other profile shapes [1,2]. Cold-formed sections offer numerous environmental advantages in construction including (a) sustainable production [3]; (b) recyclability [4]; (c) lightweight [2–5]; (d) durability [6] and (e) energy efficiency [7]. Thin cold-formed members are prone to web-crippling failure, which is localized failure that takes place when subjected to concentrated loads and reactions, as shown in Fig. 1 (b). The web crippling capacity of a Cold-Formed Steel Lipped (CFSL) channel depends on key factors such as the thickness, web height, internal bending radius, the bearing length of the loaded plate, and the material yield stress [8–10]. The cross-sectional variables of a CFSL channel are displayed in Fig. 1(a).

Considering the location of the failure and the loading conditions, contemporary standards classify web crippling load cases into two primary categories, namely one flange load cases and two flange load cases. In one flange load cases, the concentrated load is applied to the web through a single flange of the CFSL member. This can occur in various scenarios, such as when a beam is supported by a bearing plate resting on one flange or when a floor joist is loaded by a concentrated force applied to one flange. The one-flange load cases are divided into Interior-One-Flange (IOF) and End-One-Flange (EOF). In two flange load cases, the concentrated load is applied to the web through both flanges of the CFSL member simultaneously. This can occur when a beam is supported by a bearing plate resting on both flanges. The two flange load cases are divided into Interior-Two-Flange (ITF) and End-Two-Flange (ETF). This study investigates the web crippling capacity under two flange load cases, as illustrated in Fig. 2. The one flange load case is out of the scope of the study.
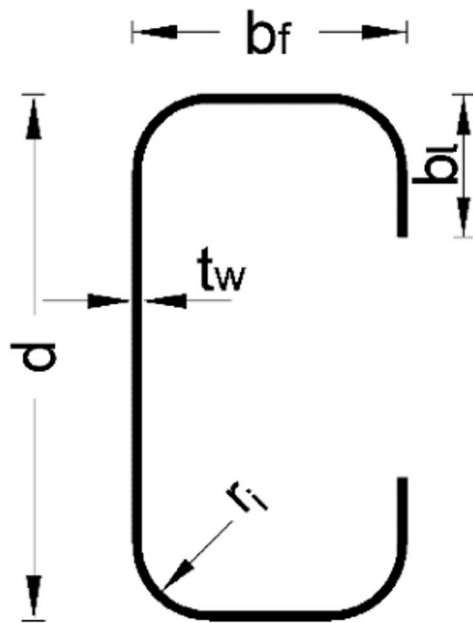
Several standards provide formulas for calculating web-crippling

---

Nomenclature

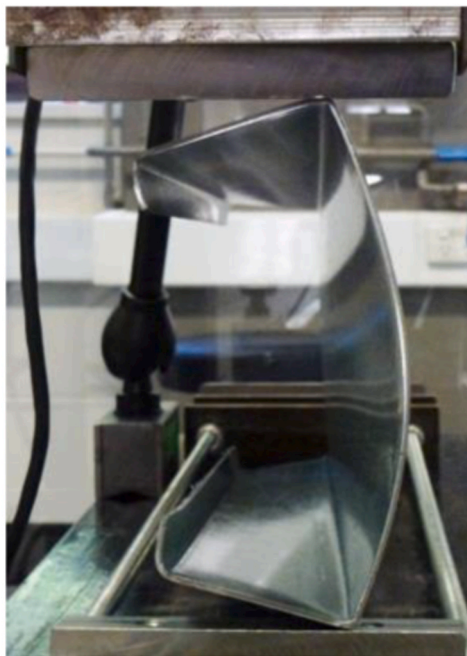|	
b_f	Flange width
b_l	Lip length
b_o	bias at the output layer
b_{hk}	bias at the hidden layer
C_r	Coefficient of internal bending radius
C_l	Coefficient of bearing length
C_w	Coefficient of web slenderness
$C_b, C_{b,r}, C_{b,l}, C_{b,w}, C_{b,b}$	Factors depends on loading condition
C_P	Correction factor
C_ϕ	Calibration factor
d	Depth of the web
d_l	Depth of the flat portion of the web
$E_{0.2}$	The tangent modulus of the stress-strain curve at the yield strength (0.2 % proof stress)
F_m	Fabrication factor
f_{sig}	sigmoid transfer function
F_y	Yield stress
$f_{y,c}$	Enhanced yield stress at corner regions
hw	The web height between the midlines of the flanges
K	Elastic buckling coefficient
M_m	Material factor
L	Channel length
l_b	Bearing length
P_m	Average ratio between the tested load and the predicted load
P_{cr}	Critical buckling load
r_{ext}	External bent radius $(r_i + t_w)$
r_i	Internal bending radius
r_m	Internal bending radius measured along the middle of the section $(r_i + 0.5t_w)$
R	Web crippling capacity
R_{norm}	Normalized web crippling capacity
S_s	Length of uniform load applied
t_w	Thickness of the web
V_F	Fabrication factor
V_M	Material factor
V_P	Variability coefficient of the tested load / predicted load
w_k	weight connection between neuron k of the hidden layer and the output neuron
w_{ik}	weight connection between input variable and neuron k of the hidden layer
x	given input parameter
X_i	input parameter i
x_n	Normalized input parameter
x_{max}	Maximum of input parameters
x_{min}	Minimum of input parameters
β_o	Parameter equal to 2.5
θ	angle between the plane of the web and the plane of the bearing surface
λ	Web crippling slenderness
ν	Poisson's ratio
$\phi, \varnothing_w$	Capacity factor

Fig. 1. CFSL channel: (a) Cross Section variables and (b) Typical web crippling failure under Interior-Two-Flange load case [10].
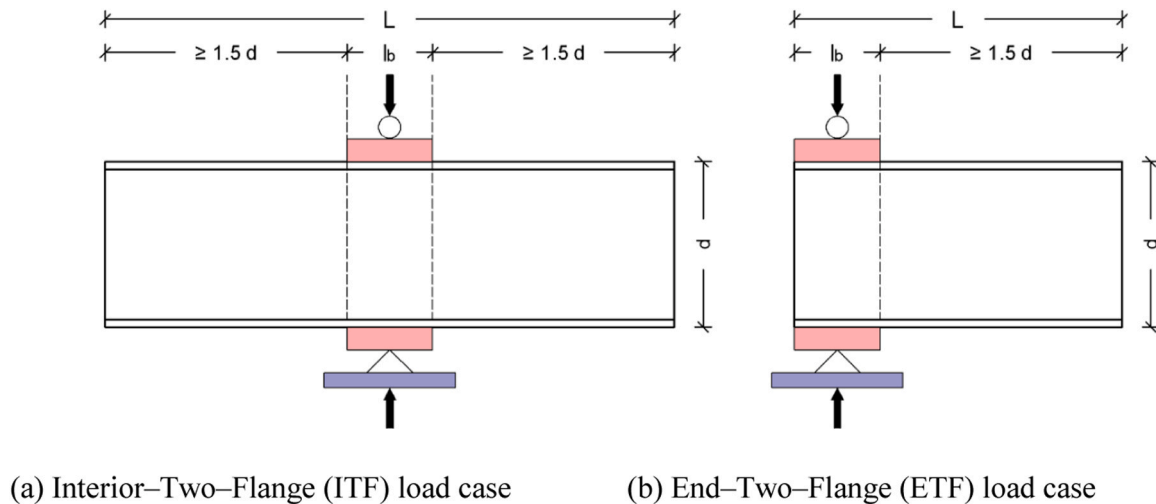
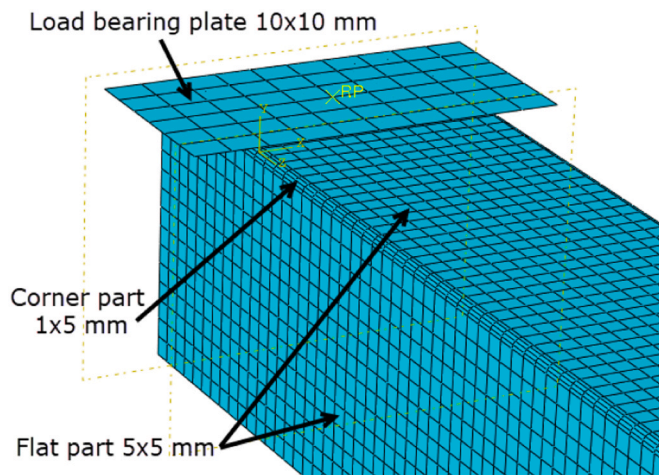**Fig. 2.** Web crippling load cases (a) ITF load case (b) ETF load case.

Fig. 3. Meshing size.

capacity of CFSL sections. EN 1993–1-3:2005 [11] uses separate equations Eqs.(13) to (18) for each load case of CFSL channels, while AISI S100–16 (R2020) [12] and AS/NZS 4600 [13] employ a single equation Eq.(19) with parameters adjusted for different loading conditions. However, Sundararajah et al. [14] found that the AISI formula could be unconservative for CFSL members. They proposed two alternative equations: Eq. (20) modifies the AISI S100–16 equation with updated factors for better agreement with test data, while Eq.(21) incorporates a new factor to account for the influence of steel grade. These equations are given in Table 8. In a channel section, the flanges and web are treated as simply supported plates [14,15].

Recently, the adoption of the Direct Strength Method (DSM) has gained prominence as a preferred approach for designing CF sections [16]. It is considered an alternative to the effective width method in design standards such as AISI S100 and AS/NZS 4600. The direct strength method differs from the effective width method by emphasizing the importance of an accurate elastic stability analysis. The buckling analysis accounts for factors such as support conditions, applied load patterns, and overall system behavior, rather than solely focusing on the individual elements that make up the cross section [15]. Current DSM design formulas Eq. (22-25) are illustrated in Table 8. However, the DSM involves complex calculations and requires a good understanding of buckling behavior. This complexity can make it challenging to implement without specialized software, especially for estimating the critical

buckling loads.

While discussing design methods like the effective width method and direct strength method for thin-walled structures, it's crucial to remember their inherent limitations. These methods are not theoretically perfect; they simplify complex non-linear problems into workable models for engineers, offering a practical design tool without demanding detailed analyses or extensive testing for every member. As a result, applying safety factors or resistance factors to these simplified models in design is essential to account for errors in their strength predictions [15].

Machine Learning (ML) techniques can be used to overcome the limitations of both the direct strength method and the effective width method. The ML models have the capability to discern complex nonlinear correlations between input and output variables. In addition, various research works have shown that artificial intelligence models provide more accurate predictions than empirical formulas. However, a large amount of data is required to train the models. In this paper, a hybrid soft computing strategy is proposed to forecast the web crippling capacity of CFSL sections subjected to two flange load cases. The strategy combines artificial neural networks (ANN) with either genetic algorithms (GA) or particle swarm optimization (PSO) to enhance efficiency and robustness in crippling capacity prediction. First, a numerical finite element (FE) model is proposed and is validated by existing test results. A comprehensive database is then created using five extracted features from experimental results to train machine learning models. Three machine learning models ANN, GA-ANN, and PSO-ANN are employed in the study. The performance of these models is evaluated. Based on the results obtained by ML algorithms, a design model is proposed and compares with current design codes.

2. Finite element analysis of CFSL channels

2.1. Element and mesh

A finite element program ABAQUS was utilized to simulate the experimental work. Natario et al. [17] explored the effectiveness of quasi-static analysis using ABAQUS/Explicit in simulating the web crippling behavior of channel sections subjected to (ETF) and (ITF) load cases. Their findings revealed that the explicit analysis delivered highly accurate predictions of experimental data in terms of ultimate load, post-collapse load-deflection behavior, and failure mechanism. Notably, the quasi-static analysis yielded a more accurate prediction of the experimentally observed failure mode than the non-linear static analysis. As a result, Explicit Quasi-static analysis was used because of its effectiveness in handling complex problems with contact and
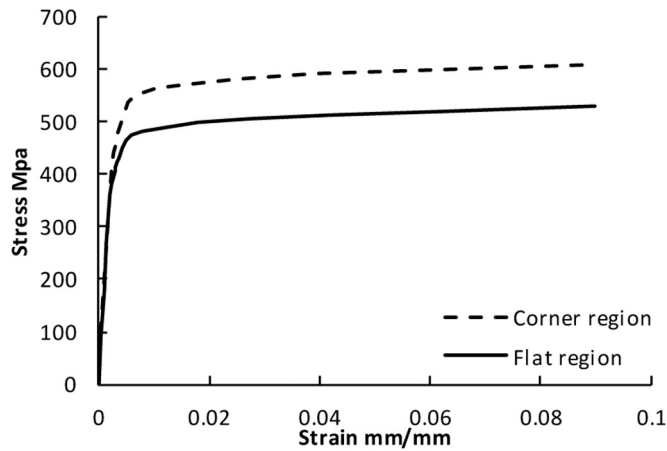
Fig. 4. Typical stress strain curves for $t_w = 1.5$ mm, $r_i = 6$ mm and $f_y = 450$ Mpa.

convergence challenges [9,18–20]. Central dimensions of CFSL channels were used in the modelling. Accordingly, the separation between the bearing plate and CFSL channels was half the thickness of the CFSL element.

The S4R shell element with reduced integration was used to model CFSL sections. The bearing plates were simulated utilizing the R3D4 quadrilateral rigid body. A rigid body was typically used to model components or structures that have much higher stiffness compared to the surrounding material, such as rigid supports, fixtures, or large masses.

Mesh refinement is crucial for obtaining accurate numerical results. As recommended in previous studies [8–10], the mesh sizes for web and flanges were 5 mm × 5 mm, and a more refined mesh with dimensions of 5 mm × 1 mm was implemented in the corner regions to facilitate the correct transmission of loads from the flange to the web, and represent the impacts of corner radius in relation to plastic deformations at the juncture of the web and flange [21]. The 10 mm × 10 mm mesh size was used for bearing plates since they do not affect web crippling performance, as shown in Fig. 3.

2.2. Material model for cold-formed steel

Multi-linear isotropic hardening material model was employed in the FE model, where the modified two-stage Ramberg-Osgood model suggested by Gardner and Yun [22] was used to simulate the stress-strain response of cold-formed steel sections. The model is expressed in mathematical form as follows:

$$\varepsilon = \begin{cases} \dfrac{f}{E} + 0.002\left(\dfrac{f}{f_y}\right)^n & f \leq f_y \\[2ex] \dfrac{f - f_y}{E_{0.2}} + \left(\varepsilon_u - \varepsilon_{0.2} - \dfrac{f_u - f_y}{E_{0.2}}\right)\left(\dfrac{f - f_y}{f_u - f_y}\right)^m + \varepsilon_{0.2} & f_y \leq f \leq f_u \end{cases} \tag{1}$$

where $E_{0.2}$ is defined as

$$E_{0.2} = \frac{E}{1 + 0.002n\frac{E}{f_y}} \tag{2}$$

The ultimate tensile strength f_u and corresponding strain ε_u are obtained from the following expressions:

$$\frac{f_u}{f_y} = 1 + \left(\frac{130}{f_y}\right)^{1.4} \tag{3}$$

$$\varepsilon_u = 0.6\left(1 - \frac{f_y}{f_u}\right) \tag{4}$$

For corner regions, Eqs.(1)–(4) utilize the following expression given by [22] to predict the enhanced yield stress $f_{y,c}$, which accounts for the effects of plastic deformations caused by cold forming of steel sections:

$$f_{y,c} = \frac{B_c}{(r_i/t_w)^a}f_y \tag{5a}$$

$$B_c = 3.69(f_u/f_y) - 0.819(f_u/f_y)^2 - 1.79 \tag{5b}$$

$$\alpha = 0.192(f_u/f_y) - 0.068 \tag{5c}$$

Typical stress-strain relationship is illustrated in Fig. 4 for flat and corner regions.

As required by the ABAQUS program, the engineering curve is transformed into the true stress and strain. The following expressions can be used:

$$\sigma_{\text{true}} = \sigma(1 + \varepsilon) \tag{6a}$$

$$\varepsilon_{\text{true}} = \ln(1 + \varepsilon) \tag{6b}$$

The strain hardening exponents n and m are 7.6 and 3.8 for flat part of the cold-formed section, respectively; however, they are taken as 7.0 and 4.2 respectively for the corners of the section [22]. The modulus of elasticity for steel material is 203,000 MPa with Poisson's ratio equal to 0.3, and the steel density is taken as 7850 kg/m³ for the explicit quasi-static analysis.
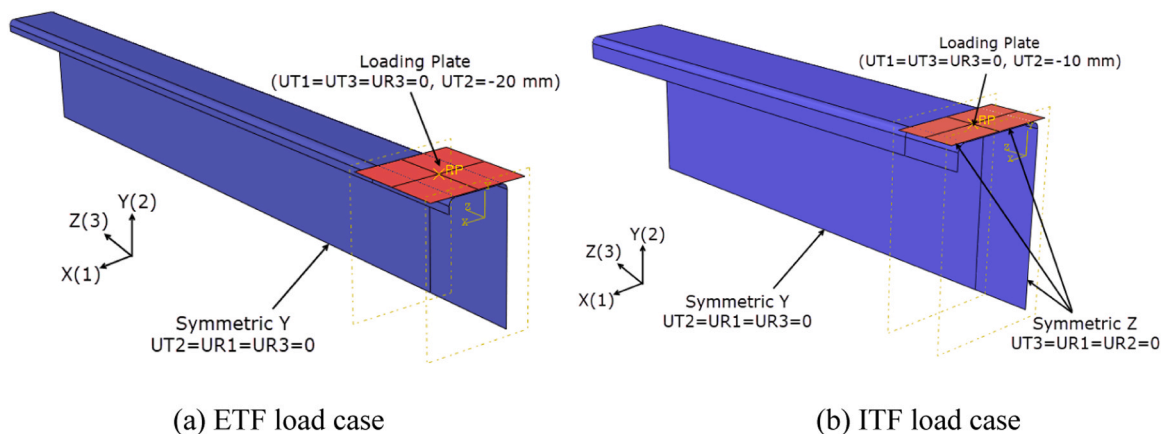

(a) ETF load case

(b) ITF load case

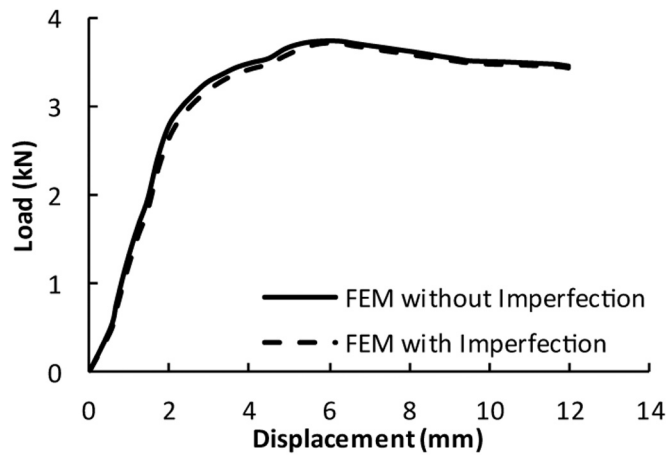**Fig. 5.** Boundary conditions (a) ETF load case (b) ITF load case.

Fig. 6. The effect of imperfection on the response of ETF150–62.5-1.52–50 channel.

2.3. Boundary conditions

Symmetry boundary conditions reduce the time for the analysis. One-half of the test set-up was modelled for the ETF load case via symmetry about the horizontal planes, as shown in Fig. 5(a). For the ITF load case, one-quarter of the model was employed using symmetry about vertical and horizontal plans as shown in Fig. 5(b).

A single reference point, which represented the rigid body components, was used to assign the boundary conditions for bearing plate. The bearing plate had free vertical movement constrained to 20 mm towards the flange, while all translations along transverse and longitudinal axes and rotations about the longitudinal axis were prevented to simulate the experimental setup. The ITF load case limited this movement to 10 mm due to the model's Z-plane symmetry. The model employed a displacement control method. A "smooth step" was assigned to the displacement amplitude to gradually apply the load during the simulation to limit the impact of the inertial influences on the FEA.

The contact between the bearing plate and the CFSL surfaces was modelled using surface-to-surface interaction using kinematic contact constraint, where the contact element was the bearing plate and the target elements were the flange plus corners. In the normal direction, hard contact was chosen to prevent the penetration of the bearing plate surface into the CFSL surface and to ensure that no contact pressure was

Table 1
Validation of FEM web crippling capacity against Sundararajah et al. [14] ETF test results.

No.	CFSL channel	l_b (mm)	f_y (MPa)	t_w (mm)	r_i (mm)	b_f (mm)	b_l (mm)	d (mm)	L (mm)	Exp (kN)	FEA (kN)	Exp/FEA
1	ETF100.4-50.5-1.03-25	25	581	1.03	3.5	50.5	13.4	100.4	306	1.76	1.72	1.02
2	ETF100-50-1.52-25	25	540	1.52	4	50	15.4	100	307	4.24	4.1	1.03
3	ETF150-62-1.21-25	25	556	1.21	4	62	19.6	150	456	2.06	2.06	1.00
4	ETF150.2-62.5-1.52-25	25	531	1.52	4.5	62.5	18.1	150.2	456	3.63	3.51	1.03
5	ETF203.7-77-1.91-25	25	506	1.91	5	77	22.1	203.7	609	5.51	5.17	1.07
6	ETF203.6-76.5-2.41-25	25	526	2.41	5	76.5	20.4	203.6	609	9.1	9.24	0.98
7	ETF100.3-50.5-1.03-50	50	581	1.03	3.5	50.5	13.6	100.3	306	1.74	1.87	0.93
8	ETF100.9-51.3-1.52-50	50	540	1.52	4	51.3	15.7	100.9	307	4.47	4.44	1.01
9	ETF150.7-61.8-1.21-50	50	556	1.21	4	61.8	19.5	150.7	456	2.23	2.19	1.02
10	ETF150-62.5-1.52-50	50	531	1.52	4.5	62.5	18.4	150	456	3.74	3.72	1.01
11	ETF203.4-76.5-1.91-50	50	506	1.91	5	76.5	21.9	203.4	609	5.63	5.41	1.04
12	ETF99.8-50.2-1.03-100	100	581	1.03	3.5	50.2	14	99.8	306	2.13	2.21	0.96
13	ETF100.4-50.9-1.52-100	100	540	1.52	4	50.9	15.3	100.4	306	5.27	5.48	0.96
14	ETF150.9-61.9-1.21-100	100	556	1.21	4	61.9	19.6	150.9	456	2.46	2.45	1.00
15	ETF150-60-1.52-100	100	531	1.52	4.5	60	19.8	150	456	4.03	4.17	0.97
16	ETF203.4-76.5-1.91-100	100	506	1.91	5	76.5	22	203.4	606	6.01	5.94	1.01
17	ETF203.5-76.4-2.41-100	100	526	2.41	5	76.4	20.4	203.5	609	9.45	10.66	0.89
Mean												1.00
COV												0.04

Table 2
Validation of FEM web crippling capacity against Sundararajah et al. [14] ITF test results.

No.	CFSL channel	l_b (mm)	f_y (MPa)	t_w (mm)	r_i (mm)	b_f (mm)	b_l (mm)	d (mm)	L (mm)	Exp (kN)	FEA (kN)	Exp/FEA
1	ITF99.9-50.6-1.03-25	25	581	1.03	3.5	50.6	14.3	99.9	510	7.05	6.61	1.07
2	ITF101.1-51.2-1.52-25	25	540	1.52	4	51.2	15.9	101.1	510	14.43	15.04	0.96
3	ITF150.3-62.1-1.21-25	25	556	1.21	4	62.1	19.6	150.3	760	9.13	8.36	1.09
4	ITF150.1-62.5-1.52-25	25	531	1.52	4.5	62.5	18.2	150.1	760	15.36	14	1.10
5	ITF203.6-76.4-1.91-25	25	506	1.91	5	76.4	22	203.6	1015	22.99	19.89	1.16
6	ITF203.7-76.6-2.41-25	25	526	2.41	5	76.6	20	203.7	1015	36.71	31.93	1.15
7	ITF100.4-50.3-1.03-50	50	581	1.03	3.5	50.3	14.5	100.4	510	6.41	6.59	0.97
8	ITF101.1-50-1.52-50	50	540	1.52	4	50	15.6	101.1	510	14.3	14.2	1.01
9	ITF151.1-62-1.21-50	50	556	1.21	4	62	18.3	151.1	760	8.16	8.06	1.01
10	ITF150.8-61.4-1.52-50	50	531	1.52	4.5	61.4	18.3	150.8	760	13.17	13.47	0.98
11	ITF203.6-76.6-1.91-50	50	506	1.91	5	76.6	22	203.6	1015	20.7	20.03	1.03
12	ITF203.6-76.7-2.41-50	50	526	2.41	5	76.7	20.6	203.6	1019	34.41	34.46	1.00
13	ITF100.1-50.7-1.03-100	100	581	1.03	3.5	50.7	13.3	100.1	510	6.45	6.68	0.97
14	ITF100.8-50.9-1.52-100	100	540	1.52	4	50.9	15.5	100.8	510	14.34	14.82	0.97
15	ITF150.4-62.3-1.21-100	100	556	1.21	4	62.3	19.6	150.4	760	8.14	8.334	0.98
16	ITF150-62.7-1.52-100	100	531	1.52	4.5	62.7	18.3	150	760	12.92	13.68	0.94
17	ITF203.1-77.3-1.91-100	100	506	1.91	5	77.3	19.4	203.1	1015	20.19	20.4	0.99
18	ITF203.6-76.7-2.41-100	100	526	2.41	5	76.7	20.2	203.6	1013	33.68	35.45	0.95
Mean												1.02
COV												0.06

Table 3

Range of input parameters.

Parameter	Symbol	Minimum	Maximum
Relative web depth	d/t_w	65	200
Relative internal bending radius	r_i/t_w	2	6
Channel thickness (mm)	t_w	1	2.4
Bearing plate length (mm)	l_b	25	150
Yield stress (MPa)	f_y	300	600

transmitted unless the nodes of the bearing plate surface contacted the CFSL surface. In the tangential direction, the friction between the bearing and the CFSL surfaces was modelled using penalty formulation and the friction coefficient was 0.4 [9,14].

2.4. Effect of imperfection

The effect of imperfection on web crippling capacity was investigated using an eigenvector field approach in finite element models with ABAQUS's * IMPERFECTION option. The imperfection magnitude was set to d_l/150 [14]. However, its impact on both web crippling capacity (less than 1 %) and the load-displacement curve was negligible, as seen in Fig. 6, justifying its exclusion from the study. This aligns with existing research neglecting initial geometric imperfections due to their minimal effect on ultimate web crippling capacity [14,23].

2.5. Validation of the FE model

Sundararajah et al. [14] conducted a series of experiments on CFSL channels that are used to validate the accuracy of the developed FEM. The geometry and mechanical properties of the test samples are given in
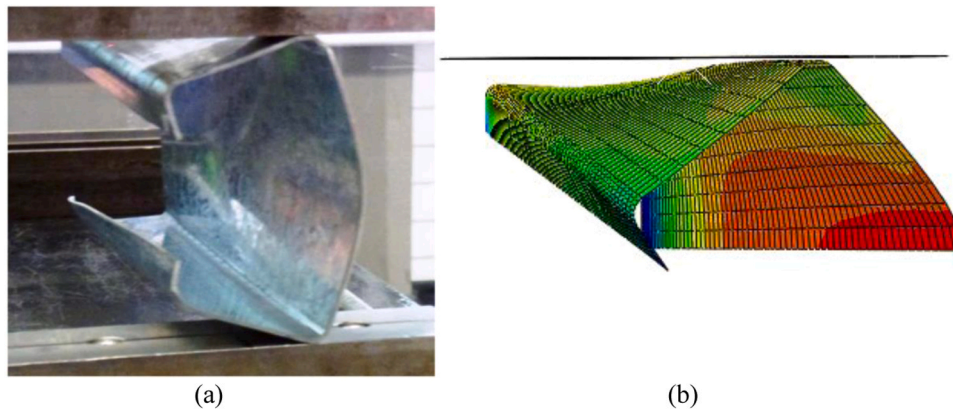

Fig. 7. Comparisons of the failure prediction of ETF100.9–51.3-1.52–50 between (a) test results observed by Sundararajah et al. [14], (b) FEA model.
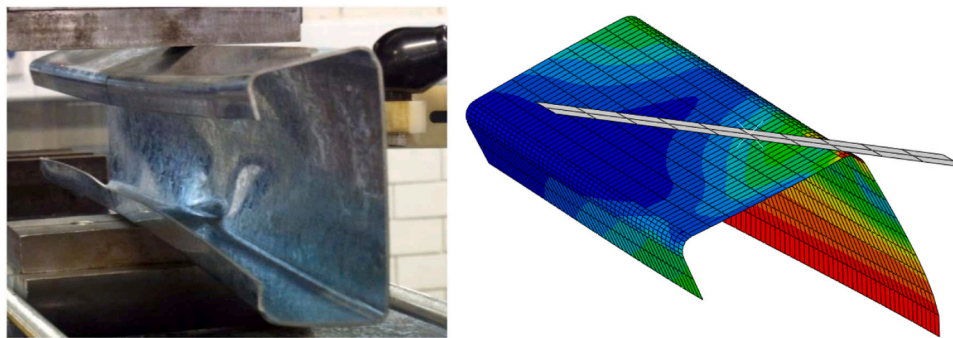

Fig. 8. Comparisons of the failure prediction of ITF101.1–50-1.52–50 by and FEA and the test results observed by Sundararajah et al. [14].
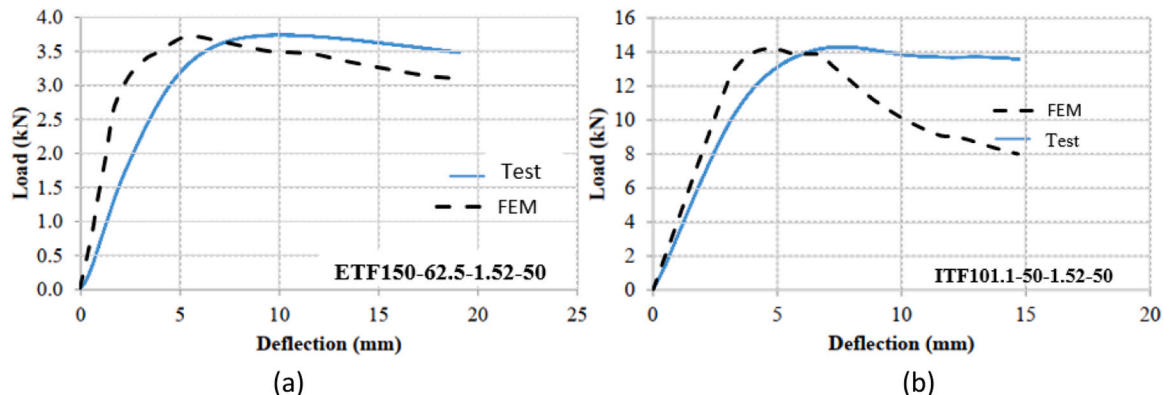

Fig. 9. Comparison of predicted and experimental load-vertical displacement curves for: (a) ETF150–62.5-1.52–50 and (b) ITF101.1–50-1.52–50.
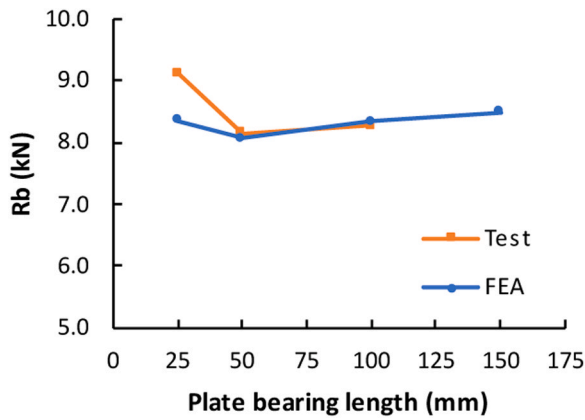
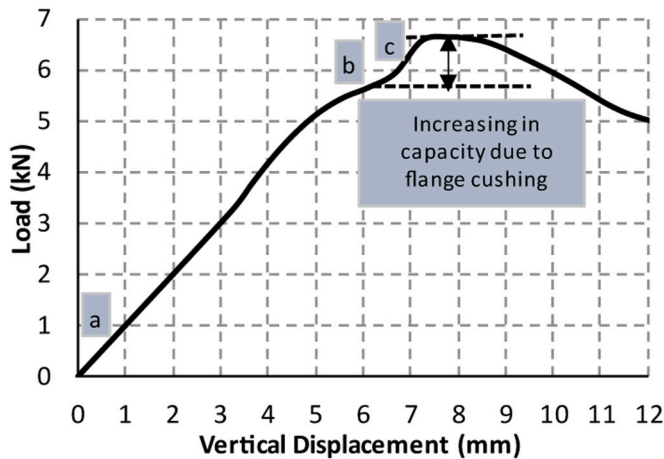**Fig. 10.** The effect of bearing length on the web crippling capacity.

Fig. 11. Load-displacement curve for ITF99.9–50.6-1.03–25.

between the test and FE simulations are shown in Fig. 7 and Fig. 8, where the contour shape refers to von mises stress. In addition, a comparison between test and FEM results of load-vertical displacement curve is illustrated in Fig. 9. The comparative study from these figures and tables demonstrates that the FEM developed for ETF and ITF load cases effectively replicates the web-crippling capacity of CFSL channels. This is substantiated by the reasonable alignment observed between the FEM results and experimental data. It is seen that the mean value of the test to prediction ratios for ETF and ITF load cases is 1.00 and 1.02, respectively, with the corresponding coefficient of variation of 0.04 and 0.06, respectively. The little discrepancies of the test and FEM results can be due to the complexity of the material behaviour, boundary conditions, and experimental uncertainties. Consequently, the proposed models can be used to conduct an extensive parametric investigation.

2.6. Parametric study

A comprehensive assessment of the web crippling capacity (denoted as Rb) in relation to changes in plate bearing length, internal bending radii, and yield stress has been meticulously conducted. The finite element analysis was undertaken on sample ITF150.3–62.1-1.21–25, ITF151.1–62-1.21–50, and ITF150.4–62.3-1.21–100. The obtained results were then compared with measurements in Fig. 10. It should be noted that the FE analysis was also performed on the sample with a bearing length of 150 mm. The findings presented in Fig. 10 clearly illustrate that the web crippling capacity increases with increasing the bearing length, except in the case of a 25 mm bearing plate. In this scenario, the ultimate load is a result of the combined effects of flange crushing and web-crippling mechanisms [14]. More specifically, Fig. 11 shows that the load-displacement relationship of the ITF99.9–50.6-1.03–25 channel exhibits two distinct phases. Initially, the response shows a proportional increase in capacity as vertical deflection develops under the bearing plate up to Point b. Beyond this peak, the shortened web depth provides greater resistance, shifting deformations toward crushing at the web-flange juncture. This flange crushing mechanism enables additional load carrying capacity [14]. Analysis indicates this post-crippling response occurs only for the 25 mm bearing length.

The effect of the internal bending radius and yield stress on the behavior of a reference CFSL channel named as ITF265–65-1.56 was investigated using the finite element analysis. The sample had a web thickness of 1.56 mm, flange width of 65 mm, lip length of 15 mm, and depth of 265 mm. The results of this analysis are presented in Fig. 12. it is observed from Fig. 12(a) that increasing the internal bending radius results in a decrease in the web crippling capacity. This can be attributed to the inverse relationship between the raised yield stress at corners and

Table 1 and Table 2. Each channel label in these tables comprises the load case followed by the depth, flange width, thickness, and plate width, respectively. Specimen dimensions followed AISI S909 guidelines with lengths equaling 3 and 5 times the web flat depth for ETF and ITF conditions respectively. Three bearing plate sizes (25, 50, 100 mm) created diverse testing conditions for both load cases. Additionally, the support system was designed to ensure that the test channels had pinned supports at both the top and bottom. The comparisons of the failure
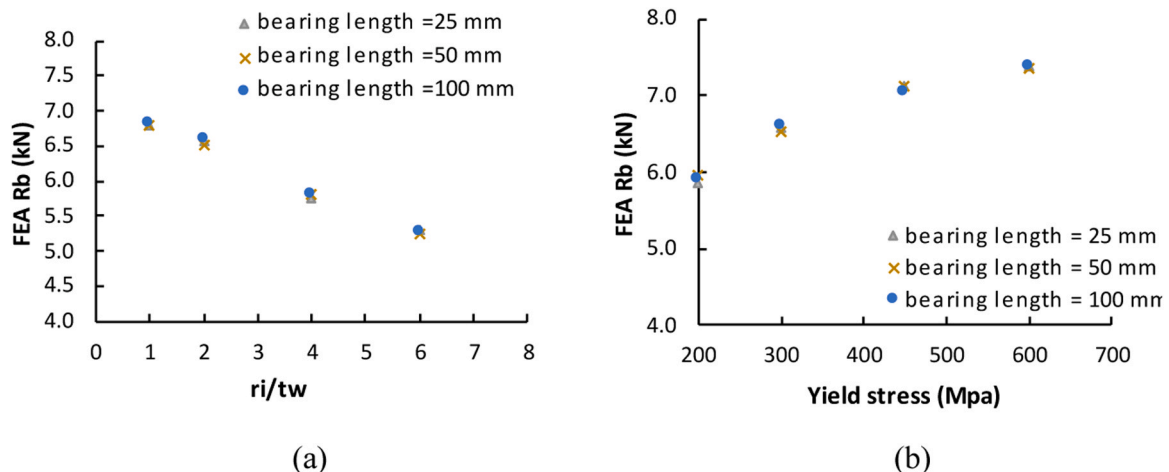

(a)

(b)

Fig. 12. The effect of influencing parameters on the web crippling capacity of ITF265–65-1.56: (a) internal bent radius/web thickness ratio, and (b) yield stress.
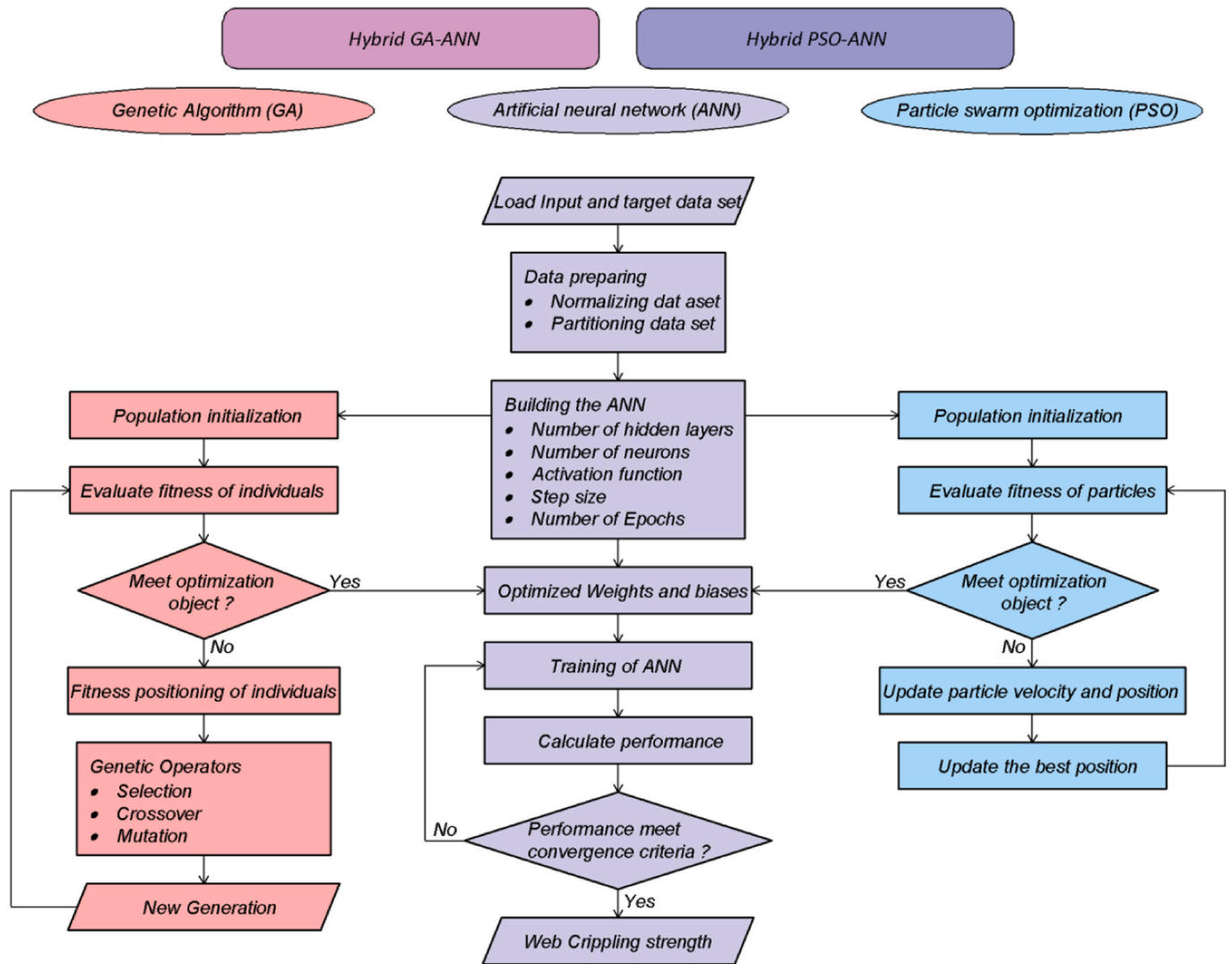
Fig. 13. Hybrid GA-ANN and PSO-ANN models.

internal bending radius, as succinctly illustrated by Eq.(5) Finally, it can be seen from Fig. 12(b) that the web crippling capacity of CFLS channels increases with increasing its yield stress.

3. Development of machine learning models

This section outlines the developed ML models and presents results from the conducted ML analysis. The conducted ML analysis leverages Artificial Neural Networks (ANN) and hypered machine learning models including Genetic Algorithm Artificial Neural Network (GA-ANN) and Particle Swarm Optimization Artificial Neural Network (PSO-ANN). The validated FE model was used to create a database containing 414 datasets for each load case. It is important to demonstrate that while finite element models provide accurate web crippling predictions, the machine learning approach offers several practical advantages. As evidenced in the prior section, properly converged finite element studies require adequate mesh size to capture the crippling behavior. This represents a computational demand beyond what is feasible for routine engineering analysis. In contrast, the machine learning model requires only basic input parameters to rapidly return buckling estimates. Additionally, constructing finite element models demands extensive expertise and time to ensure proper element choice, loading configurations, boundary conditions, and material definitions. The machine learning technique bypasses this intensive modeling preparation

through data-driven training. More importantly, common structural analysis packages tailored for engineering design typically do not contain the advanced nonlinear capabilities found in specialized research tools like ABAQUS and ANSYS. As a result, mainstream programs have not developed to handle complex instability phenomena like web crippling prediction.

3.1. Artificial neural networks (ANN)

Artificial Neural Networks (ANN) are machine learning algorithms inspired by the human brain's data processing mechanisms. ANN consists of three main components: an input layer, interconnected neurons, and an output layer. The input layer receives and passes input data to hidden layers, where computations are performed using activation functions to modify inputs before forwarding them. The output layer generates results or predictions. Neurons in different layers are linked by weights, and adjusted during training to minimize outcome disparities, often through backpropagation. ANN has been used in structural engineering previously by researchers [24–29].

Determining the optimal count of hidden layers and neurons often requires several trials to find the best network configuration [30]. Previous studies found that using one hidden layer provides acceptable accuracy for typical engineering problems [31,32]. So, one hidden layer is used in the study. The number of neurons should be sufficient to

Table 4

GA-ANN parameters.

Parameter	Value
Population size	100
Maximum number of iterations	2500
Function tolerance	1.00E-06
Crossover fraction	0.8
Migration Fraction	0.2
Migration Interval	20

Table 5

PSO-ANN parameters.

Parameter	Value
Number of particles in the swarm	100
Maximum number of iterations	2500
Function tolerance	1.00E-06
Minimum adaptive neighborhood size	0.25
Weighting of particle's best position	1.49
Weighting of the neighborhood's best position	1.49
Lower bound of the adaptive inertia	0.1
Upper bound of the adaptive inertia	1.1

precisely represent the specific problem, yet it should be kept sufficiently low to prevent overfitting of the network [33,34]. It is recommended that the optimal count of neurons in the hidden layer should not exceed twice the quantity of input points by more than one. The chosen number of neurons is based on particle swarm optimization as discussed later.

Although it provides a more accurate and reliable substitute for statistical and numerical methodologies, ANN has inherent limitations in terms of its search strategy. The optimization problem of training a neural network is often non-convex, meaning it has multiple local optima. In cases where the initial weights and biases are ill-suited, ANN may converge towards a local optimal solution, which is optimal only within a nearby subset of possible solutions, rather than reaching the global optimum. Moreover, Overfitting occurs for an excessive number of neurons because ANN becomes too complex and memorizes the training data instead of learning the underlying patterns. This can lead to different solutions when the ANN is applied to new data [14,24]. Evolutionary algorithms inspired by natural processes, such as genetic algorithms (GA) and particle swarm optimization (PSO), have displayed the potential to mitigate these constraints. Hybrid approaches combining Artificial Neural Networks (ANN) with Genetic Algorithms (GA) or Particle Swarm Optimization (PSO) have gained popularity in recent years for solving complex engineering problems such as structural optimization, damage detection, and material design [14,24,35,36].

3.2. Hybrid ANN-genetic algorithm

The Genetic Algorithm (GA) is a search-driven optimization method rooted in the principles of natural selection. GA is known for their ability to perform a global search in the solution space. They explore a wide range of potential solutions, allowing them to find optimal or near-optimal solutions even in complex and multimodal problem landscapes [37]. It works by creating a population of solutions to a given problem, which are then evaluated and rated according to a given fitness function. The solutions are then recombined and mutated over time to create new solutions, which are then evaluated and rated again. This process continues until a solution that meets the desired criteria is found. GA-ANN models combine these two approaches by using genetic algorithms to optimize the parameters of an artificial neural network.

The framework of the GA-ANN shown in Fig. 13 involves the following steps:

Problem Definition: Clearly define the optimization problem or task to be solved using the GA-ANN framework. This could include defining

the objective function. Mean Squared Error (MSE) is a popular objective function for regression problems.

(1) Encoding: Represent the ANN architecture and parameters as a chromosome $C^i = \left[w_1^i, b_1^i, w_2^i, b_2^i \right]$ where w_1^i, w_2^i are the input and output weights, respectively; b_1^i, b_2^i are the input and output biases, respectively.
(2) Initialization: Randomly initialize the initial population of chromosomes.
(3) Evaluation: Evaluate the fitness of each chromosome in the population using (MSE).
(4) Genetic Operators: Apply genetic operators, including selection, crossover, and mutation, to generate a new population of chromosomes from the existing population.
(5) Fitness Evaluation: Re-evaluate the fitness of the new population based on the updated chromosomes.
(6) Termination Criteria: Determine the termination conditions for the GA-ANN framework.
(7) Solution Extraction: Extract the best solution or chromosome from the final population.

The GA-ANN framework iteratively repeats Steps (4) to (7) until the termination criteria are met. The parameters of the GA-ANN model are presented in Table 4.

3.3. Hybrid ANN-particle swarm optimization

Particle Swarm Optimization (PSO) is a nature-inspired optimization algorithm [38]. PSO excels at global optimization tasks. It iteratively explores the search space by updating particle positions and velocities, guiding them towards the global optimum. PSO's exceptional balance between exploration and exploitation enables efficient identification of optimal or near-optimal solutions. Recent research further underscores PSO's effectiveness, particularly when combined with other optimization techniques [36,39]. PSO mimics the movement of particles or birds in a multidimensional search space to find the best solution. It operates by managing a group of particles, each representing a potential solution with position and velocity vectors. Initially, particles are randomly placed in the search space. They move iteratively, guided by their personal best and the global best positions. The movement of particles balances exploration and exploitation. Exploration involves exploring different areas of the search space by updating particle velocities based on their current state, personal best, and global best. Exploitation refines solutions by adjusting velocities toward personal and global best positions, helping particles converge toward the optimal solution. This balance is controlled by parameters like cognitive and social weights. PSO continues through iterations until a termination condition is met, like a predefined maximum number of iterations or a desired solution quality [40]. The framework of the PSO-ANN is shown in.

Fig. 13 involves the following steps:

(1) Generate a population of particles, where each particle represents a set of parameters for the neural network.
(2) For each particle in the swarm, calculate its fitness by training the corresponding neural network and evaluating its performance using an objective function.
(3) Modify the velocities and positions of the particles using their prior velocities, positions, as well as the optimal positions attained by both the individual particle and the entire swarm.
(4) Update the best positions achieved by each particle and the swarm based on the fitness values.

Repeat Steps (2−4): Iterate the process for a defined number of iterations or until a convergence criterion is met. The parameters of the PSO-ANN models are presented in Table 5.
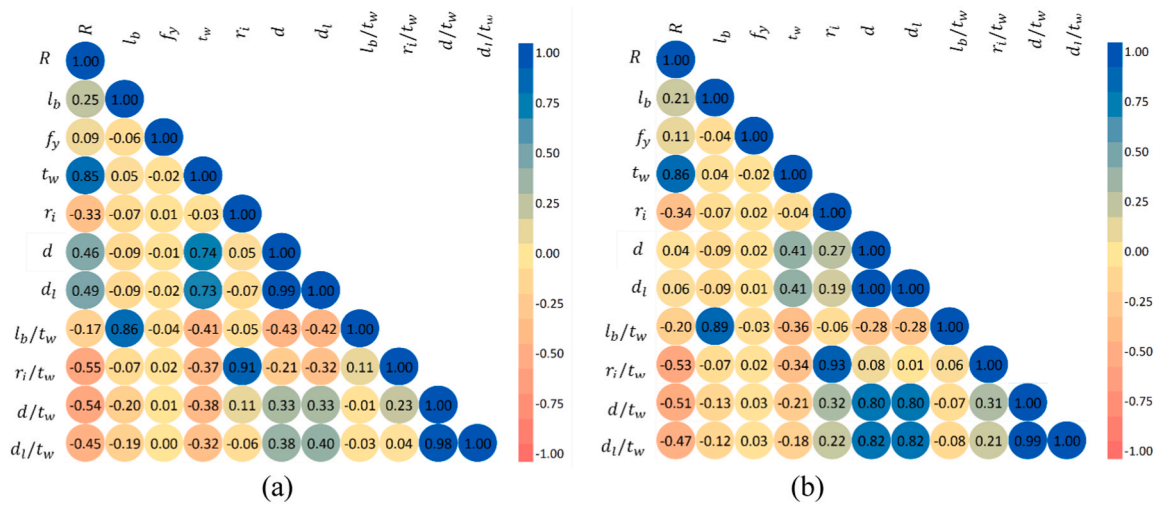
Fig. 14. Correlation matrix for suggested input variables for (a) ETF load case and (b) ITF load case.
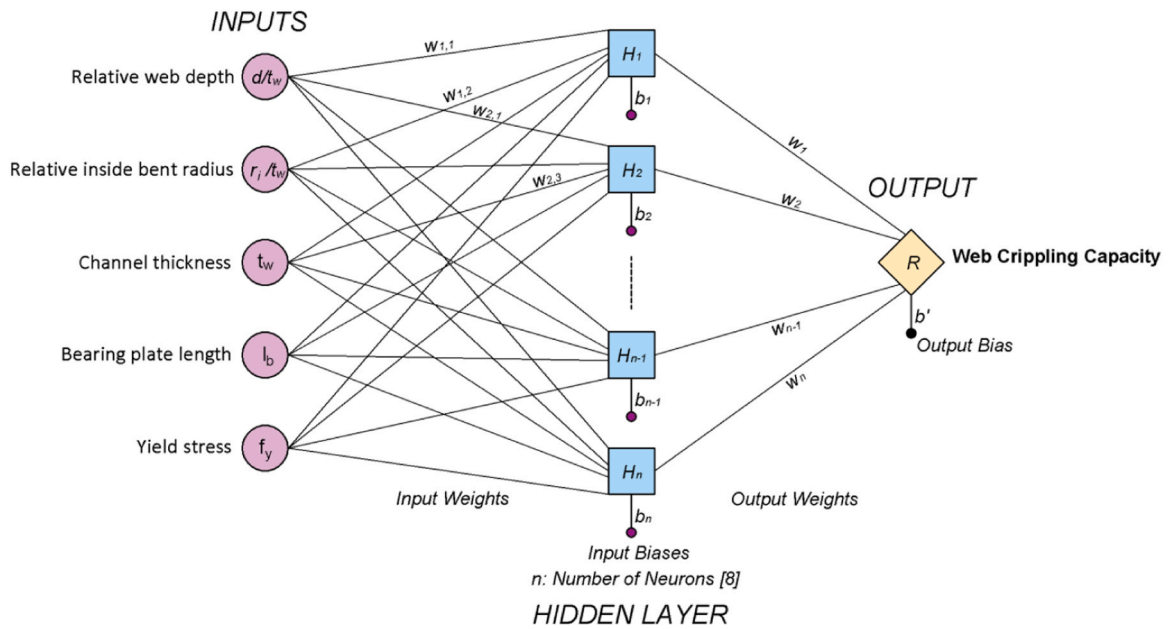

Fig. 15. Configuration of the developed ANN model.

3.4. Input parameters

In machine learning tasks, selecting the right variables for a model is crucial. One method for this is using a correlation matrix, which displays correlation coefficients between variables, ranging from − 1 (complete negative correlation) to 1 (absolute positive correlation), with 0 indicating no correlation. By examining this matrix, researchers can identify strongly correlated variables to include in their analysis. This method has been proven useful in structural engineering sensitivity analysis, providing insights into how model parameters affect responses [41].

Fig. 14 shows a correlation plot of the parameters studied. Correlation matrix is a graphical overview of the linear relationships between multiple variables in a dataset. The cells show the correlation coefficients between each pair of variables, ranging from − 1 to + 1. Values of − 1 or + 1 indicate perfect negative or positive correlation, respectively, while 0 indicates no correlation. The analysis reveals a strong positive correlation between thickness and ultimate axial load concerning the web crippling capacity. On the other side, while the correlation of the relative height d/t_w and internal bending radius r_i/t_w is

stronger than the absolute height d and internal bending radius r_i, the correlation of the absolute length of the bearing plate l_b is stronger and consistent than the relative length l_b/t_w. Besides, the correlation of the relative total height of the channel d/t_w is stronger than the correlation of the relative depth of the flat portion of the web d_l/t_w. Therefore, the section's geometry will be assessed using relative values "d/t_w, r_i/t_w", while the length of the bearing plate will be treated as an absolute value l_b. The range of input variable is shown in Table 3. The observed minor differences in the relative influence of design parameters on web crippling between (ETF) and (ITF) loading scenarios suggest that boundary condition restraint effects vary between end and intermediate locations. For ITF load case, the load is applied through both flanges at an interior location. This distribution helps spread the load across the web, reducing the localized stress concentration. But for ETF load case, the load is applied through both flanges at the end. This concentrates the load on a smaller area of the web, leading to higher stress and potential for earlier buckling. As a result, ITF sections exhibit higher strength and better stability compared to ETF sections under similar loading conditions. This variation alters how parameters like d/t_w and bearing plate
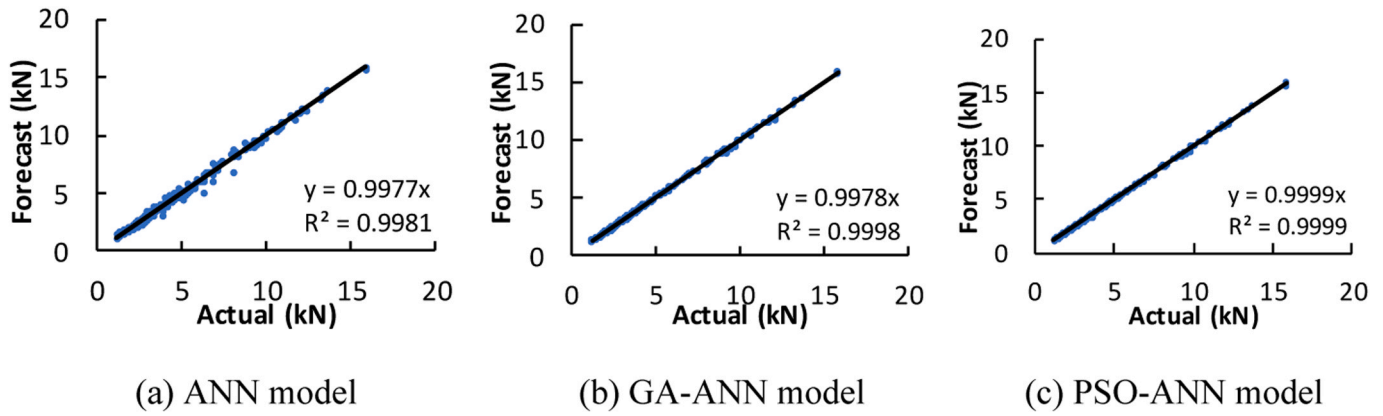
Fig. 16. Comparison of actual web crippling capacity with predicted results from ML models under ETF load case: (a) ANN model, (b) GA-ANN model, and (c) PSO-ANN model.

Fig. 17. Comparison of actual web crippling capacity with predicted results from ML models under ITF load case: (a) ANN model, (b) GA-ANN model, and (c) PSO-ANN model.
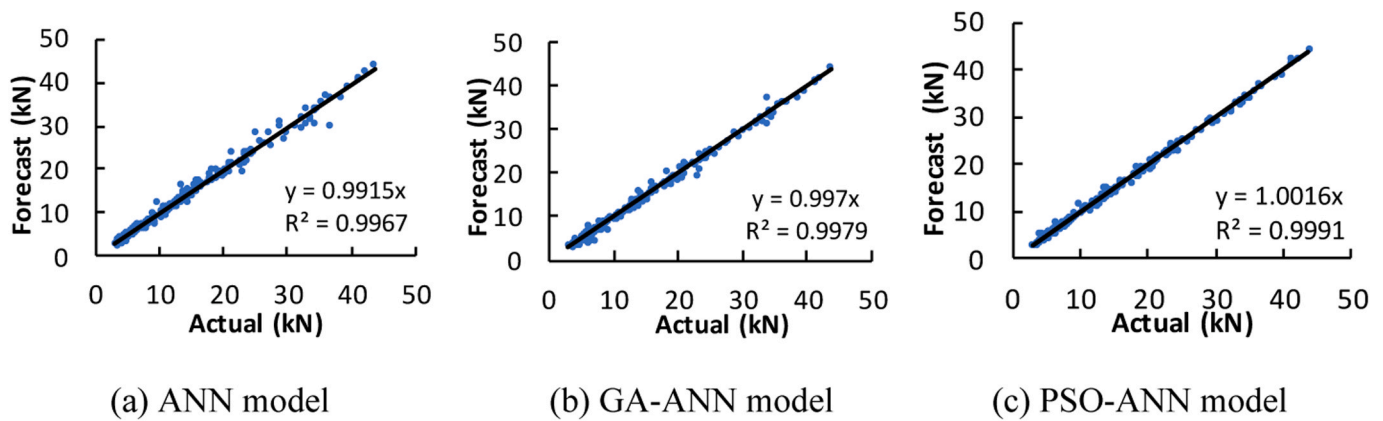
length interact to induce instabilities.

3.5. Data preparation

The second phase in constructing a machine learning model involves normalizing the dataset to improve the predictive accuracy and learning efficiency of these models. To achieve this, the linear normalization formula was utilized to rescale the independent variables within the interval [− 1, 1], employing the subsequent formula [42]:

$$X_{\text{norm}} = 2\frac{X - y}{z - y} - 1 \tag{7}$$

where y and z are the minimum and maximum values in the current list respectively. The data range is shown in Table 3. Subsequently, the dataset was randomly partitioned into three distinct subsets. Initially, a training set was created, encompassing 70 % of the records, which was employed for training the machine learning models through supervised learning. Subsequently, the remaining 30 % of the data was allocated, with 15 % serving as a validation set and the remaining 15 % as a test set. These subsets were utilized to assess the models' performance and evaluate the trained network's capacity for generalization.

The training of the dataset is carried out utilizing the Bayesian regularization backpropagation learning algorithm. The hidden layers incorporate the tan-sigmoid transfer function (tansig), while the output layer employs the linear transfer function (purelin). The assessment of network training is.

conducted through the Mean Square Error (MSE). The prescribed threshold for the maximum epochs during training corresponds to 1500. Notably, the Marquardt adjustment parameter is deliberately established at a value of 0.005.

The Particle Swarm Optimization (PSO) algorithm was employed for the purpose of optimizing the number of neurons. The range of neurons was [5–11], where 5 represents the number of parameters in the study, while 11 represents the suggested maximum number of neurons, estimated to be twice the number of variables plus 1. The Particle Swarm Optimization (PSO) algorithm was employed to search for the optimal number of neurons that achieves minimum Mean Squared Error (MSE). It was found that the appropriate number of neurons is 8. Subsequently, Artificial Neural Network (ANN), Genetic Algorithm-based Artificial Neural Network (GA-ANN), and Particle Swarm Optimization-based Artificial Neural Network (PSO-ANN) models were utilized to formulate a prediction of the web crippling capacity with high accuracy. The configuration of the developed ANN model is given in Fig. 15. Where the parameters of the GA-ANN and PSO-ANN models are presented in Table 4 and Table 5, respectively.

3.6. Performance indices

Performance assessment indices are metrics used to evaluate and quantify the performance of the model. The Correlation coefficient (R) assesses the degree of linear correspondence between the real "target" values and the projected "output" values. A correlation coefficient ranging from 0.70 to 0.89 signifies a robust correlation, while values within the range of 0.90 to 1.00 indicate an exceptionally strong correlation [9,24]. MSE, MAE, and MPE serve as metrics for gauging errors,

Table 6
Performance indices for ANN models under ETF load case.

Model	MSE	MPE	MAPE	R	a10-index
ANN	0.044	-0.314	4.439	0.997	0.908
GA-ANN	0.004	0.019	1.202	1.000	1.000
PSO-ANN	0.003	0.056	1.097	1.000	1.000

Table 7
Performance indices for ANN models under ITF load case.

Model	MSE	MPE	MAPE	R	a10-index
ANN	0.615	0.006	4.799	0.995	0.906
GA-ANN	0.378	-0.080	4.489	0.996	0.908
PSO-ANN	0.167	-0.322	2.914	0.998	0.978

and it is desirable for these values to be minimized [43].

$$R = \frac{\sum_{i=1}^{N}(t_i - \mu_T)\ (p_i - \mu_P)}{\sqrt{\sum_{i=1}^{N}(t_i - \mu_T)^2}\ \sqrt{\sum_{i=1}^{N}(p_i - \mu_P)^2}} \tag{8}$$

$$\text{MPE} = \frac{100\%}{N}\sum_{i=1}^{N}\frac{t_i - p_i}{t_i} \tag{9}$$

$$\text{MAE} = \frac{1}{N}\sum_{i=1}^{N}|t_i - p_i| \tag{10}$$

$$\text{MSE} = \sum_{i=1}^{N}\frac{(t_i - p_i)^2}{N} \tag{11}$$

where t_i and p_i are the FEA "target" and projected "output" values, respectively; μ_T and μ_P are the average values of the FEA "target" and projected "output" values, respectively; and N represents the count of values.

The $a10-$index is a performance metric that quantifies the count of data points that closely match predicted values within a permissible deviation of ± 10 % when contrasted with real-world data. The optimal score achievable is 1.0. The score range falls within the interval [0,1].

$$a10 - \text{index} = \frac{m10}{N} \tag{12}$$

where "m10" represents the quantity of data points derived from actual/predicted values, it is constrained within the range of 0.9 to 1.1.

4. Validation of ML models

The findings indicate that the trained neural networks effectively and accurately predict the web-crippling capacity of CFSL channels. It

Table 8
Empirical formulas for predicting the web-crippling capacity of lipped CFSL channels.

Source	Predictive formula		Notes
Eurocode EN 1993-1-3:2005	**End two flange (ETF)** $R_{EC-ETF} = k_1\ k_2\ k_3[6.66 - \frac{h_w/t_w}{64}][1 + 0.01\frac{S_s}{t_w}]t_w^2\ f_y/\gamma_{M1}$ **Interior two flange (ITF)**	(13)	The conditions of using Eurocode formulas are as follows: $h_w/t_w \leq 200$, $r_i/t_w \leq 6$ and $45° \leq \Theta \leq 90°$.
	$R_{EC-ITF} = k_3\ k_4\ k_5[21.0 - \frac{h_w/t_w}{16.3}][1 + 0.0013\frac{S_s}{t_w}]t_w^2\ f_y/\gamma_{M1}$ Where:	(14)	
	$k_1 = 1.33 - 0.33k$	(15)	
	$k_2 = 1.15 - 0.15r_i/t_w$ but $0.5 \leq k_2 \leq 1.0$	(16)	
	$k_3 = 0.7 + 0.3(\emptyset/90)^2$	(17)	
	$k = f_y/228; f_y$ in N/mm^2	(18)	
AISI S100-16 (R2020) and AS/NZS 4600	$R_{AISI} = Ct_w^2\ f_y\ \sin\theta\ \left(1 - C_r\ \sqrt{\frac{r_i}{t_w}}\right)\ \left(1 + C_l\ \sqrt{\frac{l_b}{t_w}}\right)\ \left(1 - C_w\ \sqrt{\frac{d_l}{t_w}}\right)$	(19)	
Sundararajah et al. [14] (1)	$R = Ct_w^2\ f_y\ \sin\theta\ \left(1 - C_r\ \sqrt{\frac{r_i}{t_w}}\right)\ \left(1 + C_l\ \sqrt{\frac{l_b}{t_w}}\right)\ \left(1 - C_w\ \sqrt{\frac{d_l}{t_w}}\right)$	(20)	factors C, C_r, C_l and C_w are given in Table 9
Sundararajah et al. [14] (2)	$R = $ $Ct_w^2\ f_y\ \sin\theta\ \left(1 - C_r\ \sqrt{\frac{r_i}{t_w}}\right)\ \left(1 + C_l\ \sqrt{\frac{l_b}{t_w}}\right)\ \left(1 - C_w\ \sqrt{\frac{d_l}{t_w}}\right)\ \left(1 - C_f\ \sqrt{\frac{250}{f_y}}\right)$	(21)	factors C, C_r, C_l, C_w and C_f are given in Table 9
Natário et al. [20,44]	$R = 0.474P_y\ \left[1 - 0.115\left(\frac{P_{cr}}{P_y}\right)^{0.728}\right]\left(\frac{P_{cr}}{P_y}\right)^{0.728}$ for ETF load case	(22)	DSM equation
	$R = \begin{cases} P_y\ for\ \lambda \leq 0.517 \\ 0.732P_y\ \left[1 - 0.156\left(\frac{P_{cr}}{P_y}\right)^{0.516}\right]\left(\frac{P_{cr}}{P_y}\right)^{0.516}\ for\ \lambda > 0.517 \end{cases}$ for ITF load case	(23)	
	$P_y = f_y\ N_m\ \left[\sqrt{4r_m^2 + t_w^2} - 2r_m\right]$		
	$N_m = l_b + 2.5r_{ext} + \frac{d_l}{2}$ for ETF load case		
	$N_m = l_b + 2\left(2.5r_{ext} + \frac{3d_l}{4}\right)$ for ITF load case		
	$r_{ext} = (r_i + t_w)$		
	$r_m = (r_i + 0.5t_w)$		
	$\lambda = \sqrt{P_{cr}/P_y}$		
Sundararajah et al. [14] (3)	$R = \begin{cases} P_y\ for\ \lambda \leq 0.71 \\ P_y\ \left[1 - 0.25\left(\frac{P_{cr}}{P_y}\right)^{1}\right]\left(\frac{P_{cr}}{P_y}\right)^{1}\ for\ \lambda > 0.71 \end{cases}$ for ETF load case	(24)	DSM equation
	$R = \begin{cases} P_y\ for\ \lambda \leq 0.94 \\ P_y\ \left[1 - 0.10\left(\frac{P_{cr}}{P_y}\right)^{0.86}\right]\left(\frac{P_{cr}}{P_y}\right)^{0.86}\ for\ \lambda > 0.94 \end{cases}$ for ITF load case	(25)	

Table 9
Coefficients for unfastened stiffened channel under two flange loading.

Factors	AISI S100 and AS/NZS 4600		Sundararajah et al. [14] (1)		Sundararajah et al. [14] (2)	
	ETF	ITF	ETF	ITF	ETF	ITF
C	13	24	5.35	17.0	1.03	1.24
C_r	0.32	0.52	0.22	0.19	0.21	0.17
C_l	0.05	0.15	0.23	0.05	0.16	0.04
C_w	0.04	0.001	0.06	0.03	0.06	0.03
C_f	–	–	-	-	6.85	16.9
$\varnothing_w$	0.90	0.80	0.76	0.82	0.85	0.88

Table 10
Factors of elastic buckling coefficient.

Load Case	C_b	$C_{b,r}$	$C_{b,w}$	$C_{b,l}$	$C_{b,b}$
ETF	0.58	0.01	0.05	0.3	0.05
ITF	1.84	0.01	0.03	0.1	0.05

should be noted that among the three machine learning models studied, the ANN model demonstrates relatively weakened predictive performance, as shown in Fig. 16(a) and Fig. 17(a). While the ANN model demonstrates the ability to accurately predict the training data, it struggles significantly when making predictions for test data. This limitation arises from the use of the conventional ANN methodology, which depends on the gradient descent technique. In situations where the training set comprises variables with numerous closely situated local minima, the model tends to converge towards local minima for error instead of the global minima.

On the other hand, the GA-ANN and PSO-ANN models exhibit strong performance in training, validation, and testing data. The majority of predictions by these models across various subsets closely align with the baseline, as depicted in Fig. 16(b), (c) for the ETF load case and Fig. 17 (b),(c) for the ITF load case. This illustrates their resilient and advantageous capability to precisely calculate the web crippling capacity of CFSL channels. The positive results they achieved underscore the advantages of employing integrated hybrid frameworks. These frameworks adeptly explore the.

potential solution space, refine the initial biases and weights within the ANN model, and ultimately reach the global optimum. However, the reliability of these models in estimating the web crippling capacity of lipped CFSL channels is heavily dependent on a comprehensive FEM database.

5. Performance assessment

It can be seen from Tables 6 and 7 that both hybrid models, GA-ANN and PSO-ANN, outperform the conventional ANN model. The *R* values for the GA-ANN and PSO-ANN models are higher than the ANN model's, indicating strong linear correlations between the predicted and actual data.

The hybrid models, GA-ANN and PSO-ANN, also show smaller values of other statistical indices, including MAPE, and MSE, confirming lower deviations and better prediction accuracy. Furthermore, the hypered models exhibit a higher A-10 index, signifying a close alignment

(a) EN1993-1-3:2005, Eq.(15)   (b) AISI S100, Eq.(19)   (c) Sundararajah et al. [14], Eq.(20)
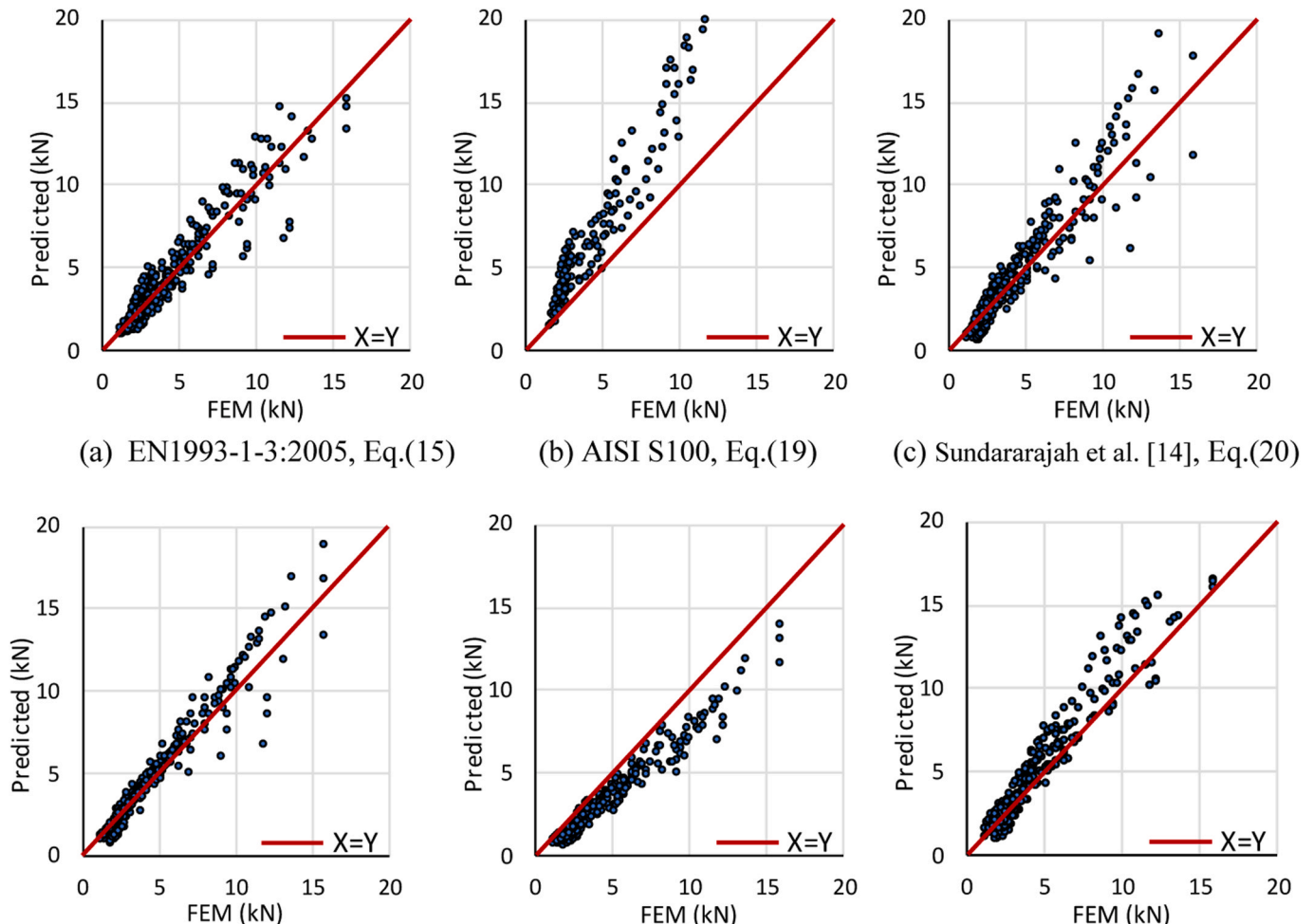
Fig. 18. Comparison of web crippling strengths obtained by formulas and FEM for ETF load case.
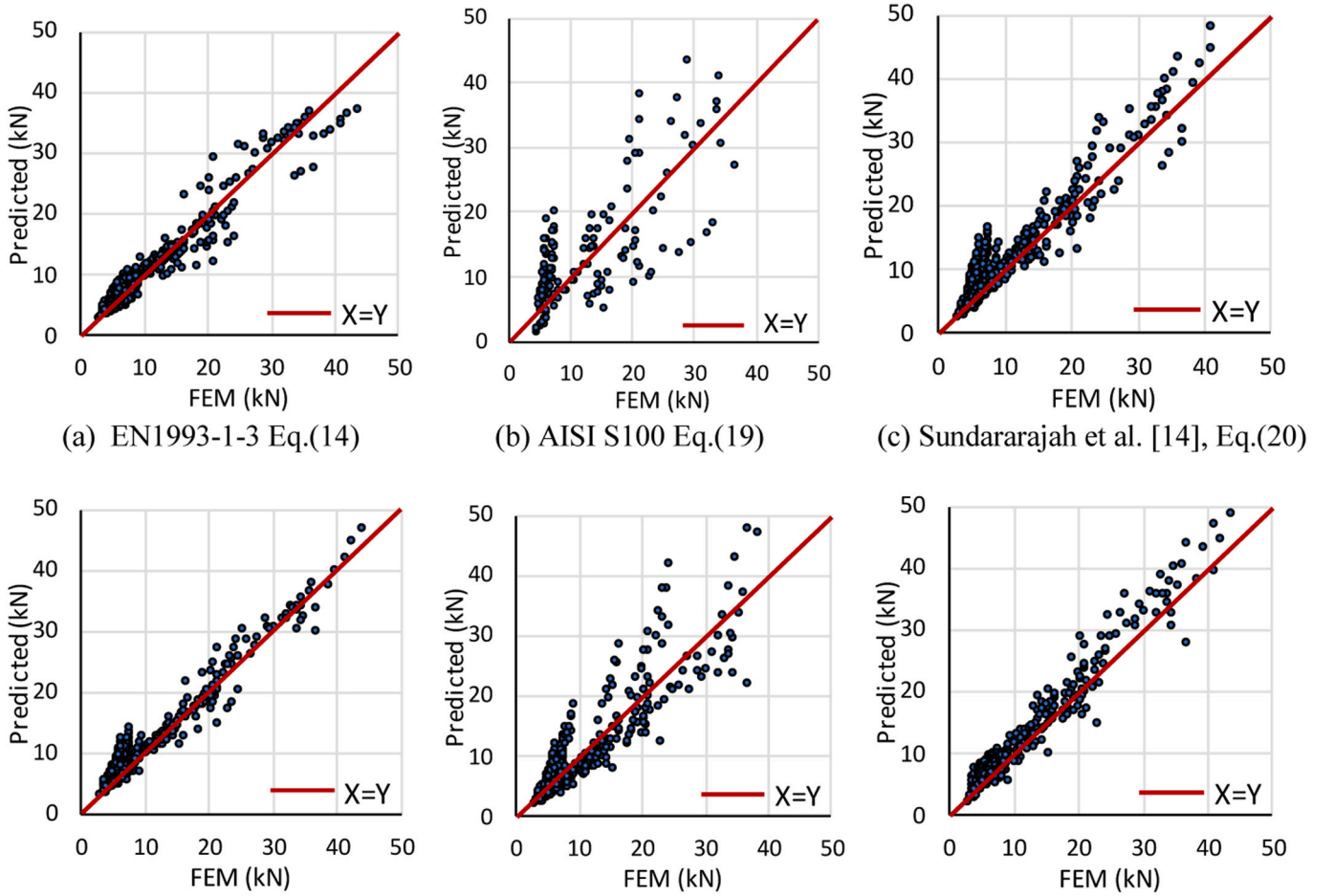
Fig. 19. Comparison of web crippling strengths obtained by formulas and FEM for ITF load case.

between the predicted values and the target values. On the other hand, the MPE results present different impressions, as they indicate that the ANN model has a lower value. However, when compared to the other performance indices and the outcomes illustrated in Table 6 for the ETF load case and Table 7 for the ITF load case, it becomes evident that this metric does not provide reliable readings for comparing artificial intelligence models, and shall not to heavily rely on it in the future. Overall, the results demonstrate the effectiveness of using hybrid models in accurately predicting the web-crippling capacity of CFSL channels.

6. Comparisons with design codes and empirical formulas

6.1. Web crippling resistance

This section examines the accuracy of the various empirical formulas specified in design codes and proposed by researchers in predicting the web crippling resistance of CFSL channels, including Eurocode EN 1993–1-3:2005, AISI S100–16 (R2020) and AS/NZS 4600 as well as the formulas proposed by Sundararajah et al. [14] and Natário et al. [20, 44]. Table 8 summarizes the empirical formulas utilized to predict the web crippling resistance for CFSL channels. In AISI S100–16 (R2020) and AS/NZS 4600, the $\frac{d_l}{t_w}$ ratio is limited to 200, and $\frac{r_i}{t_w}$ ratio is as large as 3.0 for two flanges loading cases. The condition specified in Eurocode (2005) for the applicability of its design proposal is given in Table 8.

The critical buckling load P_{cr} can be calculated using FEA programs, but the process of developing finite element models solely to calculate theoretical elastic buckling loads is often impractical from a design engineering perspective. For simplicity, the following critical buckling load equation can be used [19]:

$$P_{cr} = \frac{\pi^2}{12(1-\nu^2)} \frac{E}{d} \frac{K}{t_w^3}$$ (26)

where the following formula is suggested to estimate the elastic buckling coefficient K:

$$K = C_b \left(1 - C_{b,r} \sqrt{\frac{r_i}{t_w}}\right) \left(1 + C_{b,l} \sqrt{\frac{l_b}{t_w}}\right) \left(1 - C_{b,w} \sqrt{\frac{d_l}{t_w}}\right)$$
$$\left(1 + C_{b,b} \sqrt{\frac{b_f}{t_w}}\right)$$ (27)

Factors C_b, $C_{b,r}$, $C_{b,l}$, $C_{b,w}$, $C_{b,b}$ depend on loading conditions as shown in Table 10.

The effectiveness of previously suggested formulas in forecasting web crippling capacity under both ETF and ITF load cases, as assessed through FEM, is visually presented in Fig. 18 and Fig. 19, respectively. The figures show that for ETF load case, AISI S100 significantly overstimates the web crippling capacities of CFSL channels while the formulas suggested by Natário et al. [20,44] significantly underestimate their web crippling capacities. EN1993–1-3:2005 and Sundararajah et al. [14] provide better estimations than AISI S100 and the model of Natário et al. [20,44]; however, there is still discrepancy between the calculations and FE results. For ITF load case, the formulas suggested by Sundararajah et al. [14] provide better estimations than other design models. However, the PSO-ANN models stand out as the most accurate predictive models for web crippling capacity of CFSL channels subjected to two flange load cases.
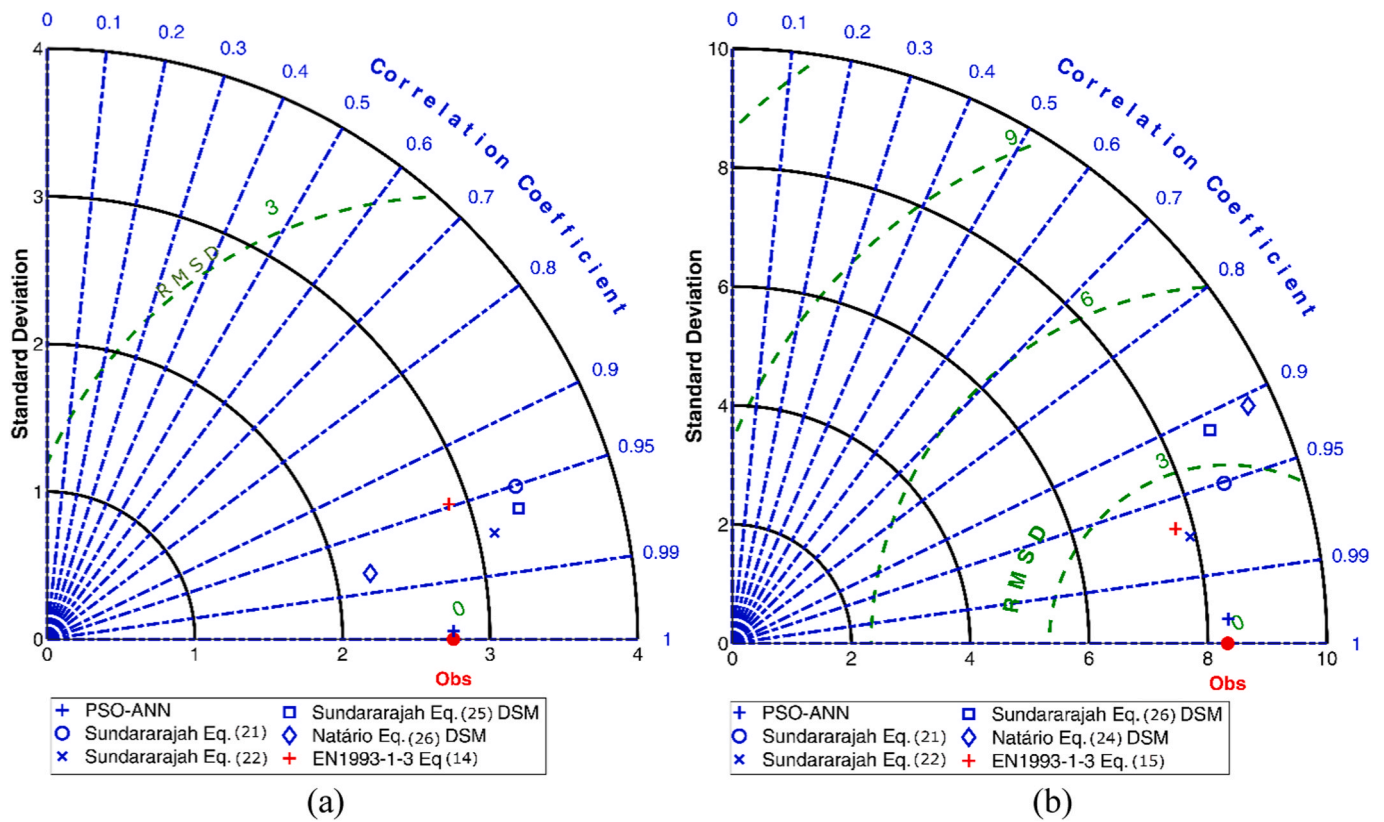
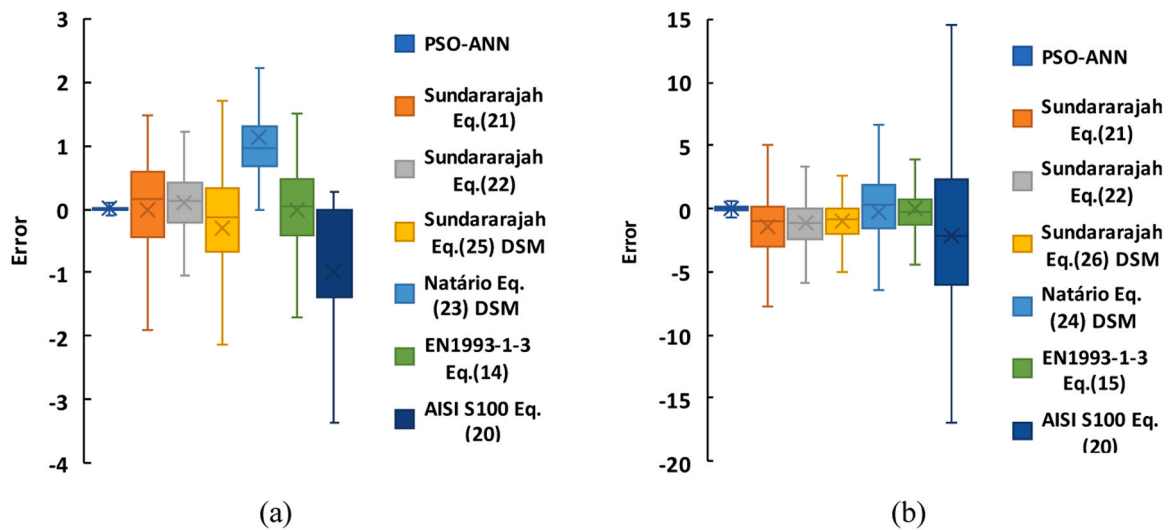**Fig. 20.** Taylor diagram of proposed ML model and past formulas under (a) ETF load case (b) ITF load case.

Fig. 21. Box plot of predictive models under a) ETF load case (b) ITF load case.

Table 11
Resistance factor $\varnothing_w$ for current and proposed formulas.

Formula	ETF	ITF
AISI S100-16 USA and Mexico	0.9	0.8
AISI S100-16 Canada	0.8	0.65
Sundararajah et al. [14] (1)	0.76	0.82
Sundararajah et al. [14] (2)	0.85	0.88
Sundararajah et al. [14] (3)	0.75	0.8
Proposed ANN model	0.9	0.9

In Fig. 20, the Taylor diagram amalgamates various statistical parameters, including Root-Mean-Square Deviation (RMSD), standard deviation, and R, derived from actual data obtained from finite element model and current formulas in addition to the proposed PSO-ANN models, facilitating direct comparisons [45]. The point labelled as "Obs" signifies the observed actual data. Notably, the proposed PSO-ANN model closely aligns with point "Obs" along the x-axis while maintaining the same standard deviation. Furthermore, the PSO-ANN model positions itself closest to the center of the RMSD circles, indicative of its superior estimation capabilities compared to other models.

A box-and-whisker plot (or boxplot) briefly visualizes the central

Table 12
The weights and biases of the proposed ANN model to determine the web crippling capacity of lipped CFSL channels subjected to ETF load case.

Neuron	Weight						Bias		Output
	Input						Output	Input	
	l_b	f_y	t_w	d/t_w	r/t_w	R_{norm}			
1	0.096	0.084	-0.285	-1.38931	-0.46372	11.194	-2.826	7.285
2	0.323	-0.270	0.326	-1.56662	-4.1679	0.769	-6.360	
3	-0.079	-0.090	0.343	1.480825	0.457936	6.067	2.613	
4	-0.087	0.056	-0.491	0.316442	0.036534	-11.887	1.524	
5	-0.086	0.070	-0.584	0.134934	0.029587	4.197	1.218	
6	-0.105	-0.060	-1.425	-0.2711	-0.04754	-0.202	-0.281	
7	0.002	10.842	-6.457	-11.8911	19.23133	-0.009	18.140	
8	-0.089	0.163	-0.434	0.528185	-0.03808	5.447	1.868	

Table 13
The weights and biases of the proposed ANN model to determine the web crippling capacity of lipped CFSL channels subjected to ITF load case.

Neuron	Weight						Bias		Output
	Input						Output	Input	
	l_b	f_y	t_w	d/t_w	r/t_w	R_{norm}			
1	-35.820	0.079	-80.842	4.675081	-2.8565	-0.561	62.068	1.774
2	0.059	14.073	-0.034	-0.10553	-0.03809	0.150	0.085	
3	2.983	0.013	-2.726	1.264749	1.091554	-0.771	5.535	
4	0.006	0.051	-0.488	0.179519	-0.00272	-2.933	-0.254	
5	0.046	0.007	14.739	-21.1027	-0.01599	0.116	8.548	
6	-0.031	-0.005	-12.677	7.708871	-0.00235	0.232	-6.779	
7	-0.054	-0.088	0.832	-0.56221	0.151386	-2.260	-1.223	
8	0.211	-0.094	0.151	-1.10754	-2.51821	3.413	-5.163	
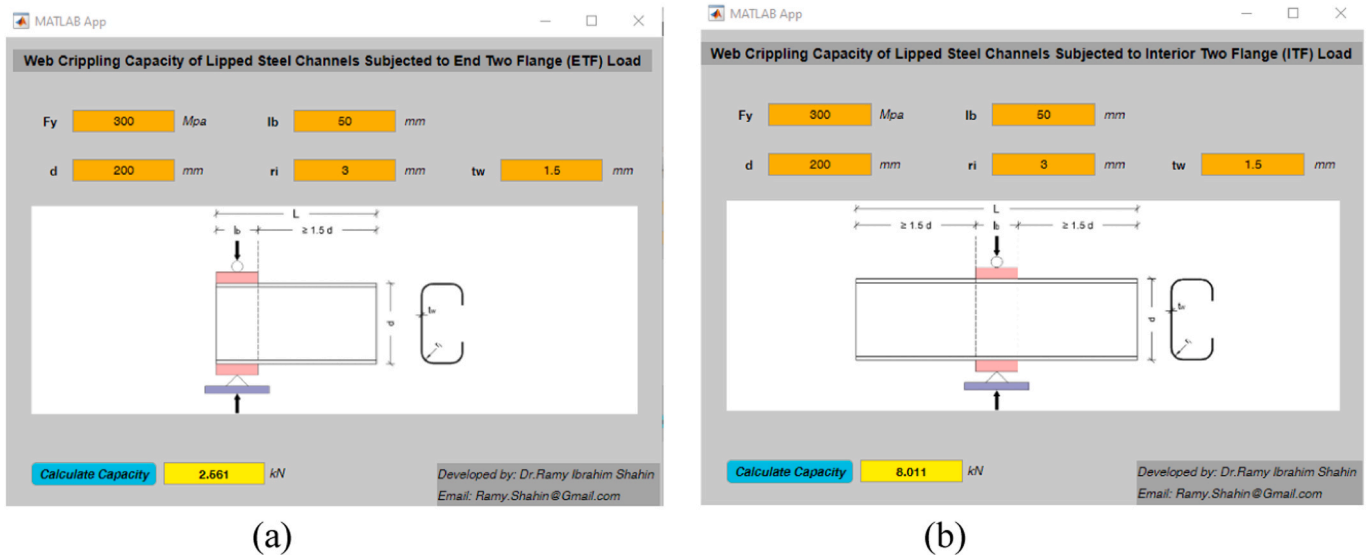
Fig. 22. Two GUI Tools to determine web crippling capacity for lipped CFSL channels subjected to two flange load cases: (a) ETF load case, and (b) ITF load case.

tendency and spread of a data set. The box represents the interquartile range (IQR), containing the middle 50 % of the data with the median bisecting it, where the bottom and top of the box show the first and third quartiles, respectively. The whiskers extend from the box capturing the majority of the remaining data points. This concise representation allows for rapid assessment of data distribution and skewness. In the context of assessing the box plot for the PSO-ANN models, notable observations emerge. Both the mean and median values (Q2) for these models closely approximate zero. Additionally, when examining the lower quartile (Q1), upper quartile (Q3), and the whiskers of the PSO-ANN models, it becomes evident that they illustrate a more limited range of errors when compared to earlier equations. This is visually represented in Fig. 21(a) for ETF load case and Fig. 21(b) for ITF load

case. These compelling findings strongly endorse the PSO-ANN models as a dependable choice for predicting the web crippling capacity of lipped cold-formed sections under ETF and ITF load cases.

6.2. Resistance factor

The AISI S100 recommends a statistical approach to determine the resistance factor used in design capacity equations, which can be used alongside the machine learning models proposed as follows:

$$\phi = C_\phi \quad (M_m \quad F_m \quad P_m) \quad e^{-\beta_o \quad \sqrt{V_M^2 + V_F^2 + C_P \quad V_P^2 + V_Q^2}} \tag{28}$$

In the LRFD method, the calibration factor C_ϕ and the load effect

factor V_Q are assigned values of 1.52 and 0.21, respectively. For members susceptible to web crippling, the material factors M_m and V_M are set to 1.1 and 0.1, respectively. The fabrication factors F_m and V_F are both established at 1.0 and 0.05, respectively. The parameter β_o is designated as 2.5 for (CF) using the LRFD method. The correction factor C_P is equal to $\frac{(1+1/n)m}{m-2}$, where n is the number of tests, and m is the degree of freedom (n – 1). P_m denotes the average value of the ratio between the tested load and the predicted load. Finally, V_P represents the variability coefficient of the ratio between the tested load and the predicted load, with a minimum threshold of 0.065.

The estimated resistance factor for ETF and ITF load cases is 0.907 and 0.914, respectively. Hence, it is advisable to employ a ϕ factor of 0.90 in conjunction with the proposed PSO-ANN models. It is important to clarify that the estimated resistance factors were derived from the validation process against the test data presented in Tables 1 and 2. These values reflect the performance of the ANN models based on the specific test data and corresponding predictions.

Table 11 presents a comparison of the resistance factor between the proposed Artificial Neural Network (ANN) model and the existing design formulas. The findings reveal that the presented ANN model produces a coefficient surpassing other models in magnitude except for AISI ETF load case for USA and Mexico. This observation implies that the presented model is highly reliable, particularly in light of its superior accuracy when compared to alternative models, as explained earlier.

7. The proposed design tools

7.1. Proposed formula

The specific formula for web crippling capacity can be directly deduced from the PSO-ANN models for daily design applications using Table 12 for ETF load case and Table 13 for ITF load case. The formula involving the input and output variables is written as [46]:

$$R_{norm} = f_{sig}\left\{ b_o + \sum_{k=1}^{h}\left[w_k \times f_{sig}\left(b_{hk} + \sum_{i=1}^{m} w_{ik} \quad X_i \right) \right] \right\} \tag{29}$$

The normalized web crippling capacity in Eq.(29) was derived by applying the weights and biases listed in Table 12 or Table 13 to the equation. It is worth to mention that the input variables should be normalized within the interval [− 1, 1] using Eq.(7). Then, the output R_{norm} can be de-normalized using Eq.(30).

$$R = \begin{cases} 7.335R_{norm} + 8.505 & \text{for ETF load case} \\ 20.395R_{norm} + 23.315 & \text{for ITF load case} \end{cases} \tag{30}$$

7.2. Graphical user interface

A practical graphical user interface (GUI) software, shown in Fig. 22, has been developed for engineers. The user can obtain the web crippling capacity by providing the input parameters shown in Fig. 22. The GUI tools can be downloaded for the ETF load case [47] and for the ITF load case [48] for free.

8. Conclusions

This paper has presented computationally efficient machine learning models for predicting the web-crippling capacity of CFSL channels subjected to two flange load cases. Finite element models have been established to assess the web crippling capacity of CFSL channels under both End Two Flange and Interior Two Flange loading conditions. A parametric study has been performed to identify the most influential parameter influencing the web crippling capacity. The validated FE models have been used to develop a database covering a wide range of important parameters. The developed database has been employed to train and test hybrid ML techniques incorporating ANN with either

genetic algorithms or particle swarm optimization (PSO) to improve the computational efficiency and accuracy of ML prediction. The accuracy of the ML results has been examined against various empirical formulas available to calculate the web crippling capacity of CFSL channels. The key findings are as follows:

1. The developed finite element models accurately predict the web crippling capacity of CFSL channels under both End Two Flange (ETF) and Interior Two Flange (ITF) loading conditions.
2. Equations (21, 24, 25) proposed by Sundararajan et al. [14] provide improved solutions compared with the design codes. However, there is still a discrepancy between the calculations and FE results.
3. The proposed (PSO-ANN) model provides excellent crippling capacity prediction compared to the existing equations, which makes it a more accurate and reliable alternative. In addition, the evaluation of predictive performance indicates the (PSO-ANN) framework achieves improved modeling accuracy over the stand-alone ANN and (GA-ANN) approaches. This is evidenced by more favorable statistical metrics like lowered mean squared error and higher correlation coefficient values for the PSO-ANN method.
4. A user-friendly graphic interface software has been developed for calculating the web crippling capacity of cold-formed steel lipped channels.

CRediT authorship contribution statement

Ramy I. Shahin: Writing – original draft, Visualization, Validation, Software, Project administration, Methodology, Investigation, Formal analysis, Data curation, Conceptualization. **Qing Quan Liang:** Writing – review & editing, Visualization. **Mizan Ahmed:** Writing – review & editing, Visualization, Methodology, Conceptualization. **Saad A. Yehia:** Writing – original draft, Visualization, Validation, Software, Project administration, Methodology, Investigation, Formal analysis, Data curation, Conceptualization.

Declaration of Competing Interest

All authors certify that they have NO affiliations with or involvement in any organization or entity with any financial interest (such as honoraria; educational grants; participation in speakers' bureaus; membership, employment, consultancies, stock ownership, or other equity interest; and expert testimony or patent-licensing arrangements), or non-financial interest (such as personal or professional relationships, affiliations, knowledge or beliefs) in the subject matter or materials discussed in this manuscript.

Data availability

Data will be made available on request.

References

[1] Ma W, Becque J, Hajirasouliha I, Ye J. Cross-sectional optimization of cold-formed steel channels to Eurocode 3. Eng Struct 2015;101:641–51.
[2] Wang B, Gilbert BP, Molinier AM, Guan H, Teh LH. Shape optimisation of cold-formed steel columns with manufacturing constraints using the Hough transform. Thin Walled Struct 2016;106:75–92.
[3] Thirunavukkarasu K, Kanthasamy E, Gatheeshgar P, Poologanathan K, Rajanayagam H, Suntharalingam T, et al. Sustainable performance of a modular building system made of built-up cold-formed steel beams. Buildings 2021;11(10): 460.
[4] Liang H, Roy K, Fang Z, Lim JB. A critical review on optimization of cold-formed steel members for better structural and thermal performances. Buildings 2022;12 (1):34.
[5] Weerasinghe H, Konthesingha C, Nanayakkara A, Poologanathan K, Perampalam G, Kanthasamy E. Web crippling behaviour of cold-formed carbon steel, stainless steel, and aluminium lipped channel sections with web openings. Buildings 2022;12(11):1820.
[6] AISI. Durability of cold-formed steel framing members 4 design guide. USA: American Iron and Steel Institute; 2004.

[7] Abreu J., Punati N., Prasad K., Schafer B., Advanced modeling of cold-formed steel walls under fire. In: Proceedings of the international specialty conference on cold-formed steel structures. 4., Baltimore, Maryland, U.S.A, November 9–10; 2016.

[8] McIntosh A, Gatheeshgar P, Gunalan S, Kanthasamy E, Poologanathan K, Corradi M, et al. Unified approach for the web crippling design of cold-formed channels: carbon steel, stainless steel and aluminium. J Build Eng 2022;51:104134.

[9] McIntosh A, Gatheeshgar P, Poologanathan K, Gunalan S, Navaratnam S, Higgins C. Web crippling of cold-formed carbon steel, stainless steel, and aluminium channels: investigation and design. J Constr Steel Res 2021;179: 106538.

[10] Sundararajah L. Web crippling studies of cold-formed steel channel beams (experiments, numerical analyses and design rules). Queensland University of Technology; 2017.

[11] Eurocode 3. Design of steel structures-part 1-1: general rules and rules for buildings. Brussels, Belgium: European Committee for Standardization (CEN); 2005.

[12] AISI S100–16, North American specification for the design of cold-formed steel structural members (reaffirmed 2020) with supplement 3. Washington, DC, USA; 2022.

[13] AS/NZS 4600-2018. Cold-formed steel structures. Sydney, NSW, Australia: Australian/New Zealand Standard; 2001.

[14] Sundararajah L, Mahendran M, Keerthan P. New design rules for lipped channel beams subject to web crippling under two-flange load cases. Thin Walled Struct 2017;119:421–37.

[15] Ziemian RD. Guide to stability design criteria for metal structures. John Wiley & Sons; 2010.

[16] Ye J, Meza FJ, Hajirasouliha I, Becque J, Shepherd P, Pilakoutas K. Experimental investigation of cross-sectional bending capacity of cold-formed steel channels subject to local-distortional buckling interaction. J Struct Eng 2019;145(7): 04019064.

[17] Natário P, Silvestre N, Camotim D. Web crippling failure using quasi-static FE models. Thin Walled Struct 2014;84:34–49.

[18] Kaitila O. Web crippling of cold-formed thin-walled steel cassettes. Helsinki University of Technology; 2004.

[19] Sundararajah L, Mahendran M, Keerthan P. Experimental studies of lipped channel beams subject to web crippling under two-flange load cases. J Struct Eng 2016;142 (9):04016058.

[20] Natário P, Silvestre N, Camotim D. Web crippling of beams under ITF loading: a novel DSM-based design approach. J Constr Steel Res 2017;128:812–24.

[21] Prabakaran K. , Schuster R., Web crippling of cold formed steel members. In: Proceedings of the CCFSS proceedings of international specialty conference on cold-formed steel structures; 1998.

[22] Gardner L, Yun X. Description of stress-strain curves for cold-formed steels. Constr Build Mater 2018;189:527–38.

[23] Janarthanan B, Mahendran M, Gunalan S. Numerical modelling of web crippling failures in cold-formed steel unlipped channel sections. J Constr Steel Res 2019; 158:486–501.

[24] Chaabene WB, Flah M, Nehdi ML. Machine learning prediction of mechanical properties of concrete: critical review. Constr Build Mater 2020;260:119889.

[25] Ci J, Ahmed M, Tran V-L, Jia H, Chen S. Axial compressive behavior of circular concrete-filled double steel tubular short columns. Adv Struct Eng 2021. 13694332211046345.

[26] Phan V-T, Tran V-L, Nguyen V-Q, Nguyen D-D. Machine learning models for predicting shear strength and identifying failure modes of rectangular RC columns. Buildings 2022;12(10):1493.

[27] Tran V-L, Kim J-K. Revealing the nonlinear behavior of steel flush endplate connections using ANN-based hybrid models. J Build Eng 2022;57:104878.

[28] Asteris PG, Lemonis ME, Le T-T, Tsavdaridis KD. Evaluation of the ultimate eccentric load of rectangular CFSTs using advanced neural network modeling. Eng Struct 2021;248:113297.

[29] Le T-T, Asteris PG, Lemonis ME. Prediction of axial load capacity of rectangular concrete-filled steel tube columns using machine learning techniques. Eng Comput 2021:1–34.

[30] Cachim PB. Using artificial neural networks for calculation of temperatures in timber under fire loading. Constr Build Mater 2011;25(11):4175–80.

[31] Golafshani EM, Rahai A, Sebt MH, Akbarpour H. Prediction of bond strength of spliced steel bars in concrete using artificial neural network and fuzzy logic. Constr Build Mater 2012;36:411–8.

[32] Haddad R, Haddad M. Predicting fiber-reinforced polymer–concrete bond strength using artificial neural networks: a comparative analysis study. Struct Concr 2021; 22(1):38–49.

[33] Atici U. Prediction of the strength of mineral admixture concrete using multivariable regression analysis and an artificial neural network. Expert Syst Appl 2011;38(8):9609–18.

[34] Shahin RI, Ahmed M, Yehia SA, Liang QQ. ANN model for predicting the elastic critical buckling coefficients of prismatic tapered steel web plates under stress gradients. Eng Struct 2023;294:116794.

[35] Santarsiero G, Mishra M, Singh MK, Masi A. Structural health monitoring of exterior beam–column subassemblies through detailed numerical modelling and using various machine learning techniques. Mach Learn Appl 2021;6:100190.

[36] Chakali Y, Sadok AH, Tahlaiti M, Nacer T. A PSO-ANN intelligent hybrid model to predict the compressive strength of limestone fillers roller compacted concrete (RCC) to build dams. KSCE J Civ Eng 2021;25(8):3008–18.

[37] Katoch S, Chauhan SS, Kumar V. A review on genetic algorithm: past, present, and future. Multimed Tools Appl 2021;80:8091–126.

[38] Wang D, Tan D, Liu L. Particle swarm optimization algorithm: an overview. Soft Comput 2018;22:387–408.

[39] Li Z, Qi J, Hu Y, Wang J. Estimation of bond strength between UHPC and reinforcing bars using machine learning approaches. Eng Struct 2022;262:114311.

[40] Li L, Liu F, Li L, Liu F. Application of particle swarm optimization algorithm to engineering structures. Group Search Optim Appl Struct Des 2011:7–20.

[41] Varlamov A., Yakobchuk D., Lozhkin I., Choice of factors modelling of concrete. In: Proceedings of the IOP conference series: materials science and engineering, 2019, 661(1): IOP Publishing, p. 012087.

[42] Matlab. Choose neural network input-output processing functions. MathWorks; 2023. ⟨https://www.mathworks.com/help/deeplearning/ug/choose-neural-network-input-output-processing-functions.html⟩.

[43] Schober P, Boer C, Schwarte LA. Correlation coefficients: appropriate use and interpretation. Anesth Analg 2018;126(5):1763–8.

[44] Natário P, Silvestre N, Camotim D. Direct strength prediction of web crippling failure of beams under ETF loading. Thin Walled Struct 2016;98:360–74.

[45] Taylor KE. Summarizing multiple aspects of model performance in a single diagram. J Geophys Res Atmos 2001;106(D7):7183–92.

[46] Goh AT, Kulhawy FH, Chua C. Bayesian neural network analysis of undrained side resistance of drilled shafts. J Geotech Geoenviron Eng 2005;131(1):84–93.

[47] Shahin R.I.Crippling ETF.zip·RamyShahin/ETF_Crippling at main. Available from: ⟨https://huggingface.co/spaces/RamyShahin/ETF_Crippling/blob/main/Crippling %20ETF.zip⟩. [Accessed 2023]. 2023.

[48] Shahin R.I.Crippling ITF.zip·RamyShahin/ITF_Crippling at main. Available from: ⟨https://huggingface.co/spaces/RamyShahin/ITF_Crippling/blob/main/Crippling %20ITF.zip⟩. [Accessed 2023]. 2023.